Adhesion Assay—Confluent HAECs seeded on 24-well plates were treated with 10 μg/ml LTA for 60 min. The culture medium was then removed, and monocytic THP-1 cells (2.5×10^5) prelabeled with Alexa564-conjugated concanavalin A were added to the culture. Cells were then allowed to adhere for 30 min on a rocking platform. After two washes with phosphate-buffered saline, fluorescent images were immediately obtained by a fluorescent microscope IX71 with DP70 image capture (Olympus) and processed using Adobe Photoshop, version 7.0. Adhesion of red fluorescent cells was quantified in three fields per well. Results are representative of three separate experiments and expressed as means ± S.D.

Immunofluorescence of VWF—Confluent HAECs were treated with 10 μg/ml LTA or 10 μM A23187 for 60 min. The culture media were removed, and the cells were immediately fixed at −20 °C with methanol for 60 min. Immunostaining was carried out using an anti-VWF rabbit polyclonal antibody (Santa Cruz Biotechnology, Santa Cruz, CA) and Alexa488-conjugated secondary antibody (Invitrogen). Cell nuclei were also stained with 2.5 μg/ml Höechst 33342 for 30 min. Images were obtained by a fluorescent microscope IX71 (magnification: ×40) with DP70 image capture (Olympus) in the presence of the Prolong Gold Antifade reagent (Invitrogen) and processed using Adobe Photoshop, version 7.0 (Adobe). Results are representative of three separate experiments.

Immunoblot Analysis—Confluent HAECs seeded on 60-mm plates were transfected with gene-specific siRNA and incubated in Opti-Mem I media containing 5% fetal bovine serum for 4–6 h. The cells were stimulated with 1 μg/ml LTA for 0–60 min and lysed with a buffer consisting of 20 mM Tris-hydrochloride (pH 7.2), 150 mM sodium chloride, 5 mM EDTA, and 1% Triton X-100 in the presence of protease inhibitors (Roche Applied Science) at 4 °C for 15 min followed by clarification by centrifugation at 12,000 × *g* for 10 min. SDS-PAGE and immunoblot analyses were performed as described previously (17, 20). Results are representative of three separate experiments.

Flow Cytometry—To assess the surface expression of P-selectin, confluent HAECs were treated with 10 μg/ml LTA for 30 min. To assess the surface expression of TLR2, confluent HAECs or HUVECs were treated with 10 ng/ml IFN-γ or they were incubated for 12 h under laminar flow. Cell culture under laminar flow was performed with a cone and plate apparatus as described previously (22). Magnitude of the flow was controlled at ~15 dyn/cm^2. The cells were then removed with phosphate-buffered saline containing 20 mM EDTA and fixed with phosphate-buffered saline containing 4% paraformaldehyde at 4 °C for 60 min. The cells were then incubated at 4 °C for 60 min with anti-TLR2 monoclonal antibody (IMG-319), anti-P-selectin monoclonal antibody (BD Biosciences), or isotype-matched mouse IgG and then with fluorescein isothiocyanate-conjugated anti-mouse IgG. Fluorescence was measured using a FACSCalibur (BD Biosciences).

Statistics—All values were evaluated by statistical analysis using one-way analysis of variance and Student-Newman-Keul's test. Differences were considered to be statistically significant at the level of $p < 0.05$.

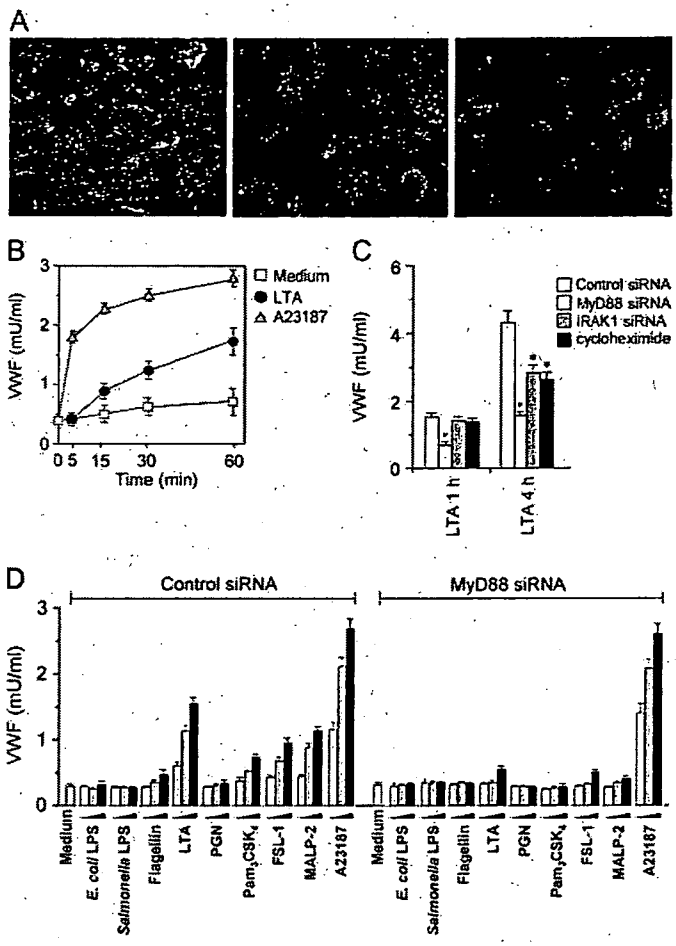

FIGURE 1. **MyD88-dependent Weibel-Palade body exocytosis by bacterial constituents.** *A*, HAECs stimulated with 10 μg/ml LTA or 1 μM A23187 for 60 min were fixed and stained immunofluorescently with anti-VWF antibody (*green*) and with Höechst33342 (*blue*). *Left*, unstimulated; *middle*, stimulated with LTA; *right*, stimulated with A23187. *B*, HAECs were stimulated with 1 μg/ml LTA or 1 μM A23187 for the indicated periods. The amounts of VWF released into the media were measured by ELISA. Each value is the mean ± S.D. ($n = 3$). *C*, HAECs transfected with MyD88 or IRAK1-specific or control siRNA were prepared. Cells were pretreated with 10 μg/ml cycloheximide for 30 min and then washed and stimulated with 10 μg/ml LTA for 60 min or 4 h. The amounts of VWF released into the media were measured by ELISA. Each value is the mean ± S.D. ($n = 3$). *, *versus* control group, $p < 0.01$. *D*, HAECs transfected with MyD88-specific or control siRNA were stimulated with *E. coli* LPS O26:B6 (0.01–1 μg/ml), LPS from *S. minnesota* (0.01–1 μg/ml), flagellin from *S. typhimurium* (0.1–10 μg/ml), LTA from *S. aureus* (0.1–10 μg/ml), PGN from *S. aureus* (0.1–10 μg/ml), Pam_3CSK_4 (0.1–10 μg/ml), FSL-1 (0.01–1 μg/ml), MALP-2 (0.01–1 μg/ml), and A23187 (0.1–10 μM) for 60 min, and then the amounts of VWF released into the media were measured. Each value is the mean ± S.D. ($n = 3$).

RESULTS

Induction of Weibel-Palade Body Exocytosis by Bacterial Constituents—We first examined whether bacterial LTA activated degranulation of Weibel-Palade bodies, because LTA has been reported to stimulate vascular endothelial cells, leading to induction of production of proinflammatory mediators, dysfunction, or cell death (23–25). After stimulation of HAECs for 30 min, LTA clearly decreased the amount of Weibel-Palade bodies, stained with an antibody to VWF, in the cells (Fig. 1*A*). Compared with the calcium ionophore (A23187)-induced response, we found that LTA gradually activated Weibel-Palade body exocytosis, quantification of which was performed by measuring the amount of VWF released into the media (Fig. 1*B*). VWF release by stimulation with

LTA for 60 min was not suppressed by treatment with the protein synthesis inhibitor cycloheximide, whereas the release by stimulation with LTA for 4 h was significantly suppressed by the treatment (Fig. 1*C*). We further investigated whether LTA induction of exocytosis was mediated through MyD88 and IRAK-1, common signaling molecules downstream of TLRs, because LTA is known as a TLR2 agonist. Interestingly, VWF release by stimulation with LTA for 60 min was suppressed by knockdown of the expression of MyD88 but not that of IRAK-1, whereas the release by stimulation with LTA for 4 h was significantly suppressed by each knockdown of MyD88 and IRAK-1 (Fig. 1*C*). Thus, these results suggest that LTA can induce Weibel-Palade body exocytosis through a MyD88-dependent rapid mechanism without *de novo* protein synthesis and an IRAK-1-dependent slower mechanism with *de novo* protein synthesis.

We also examined whether other bacterial cell wall constituents, as shown in Table 1, activated induction of VWF release after stimulation of HAECs for 60 min. Among the compounds that we tested, the synthetic analogs of bacterial lipoproteins Pam_3CSK_4, FSL-1, and MALP-2 and, to a lesser extent, flagellin induced VWF release in a dose-dependent manner (Fig. 1*D*, *left*). Interestingly, LPS from different bacterial species and PGN did not activate Weibel-Palade body exocytosis (Fig. 1*D*, *left*). In addition, we found that induction of exocytosis by bacterial compounds was also mediated by MyD88 as well as that by LTA (Fig. 1*D*, *right*). These results suggest that several types of, but not all, bacterial cell wall constituents can activate induction of TLR-MyD88-mediated exocytosis.

TABLE 1
Bacterial cell wall constituents used in this study

Substance	Origin (Ref.)	TLR recognition in human cells (Ref.)
LTA	*S. aureus*	TLR2 (7)
LPS	*E. coli*	TLR4 (10)
LPS	*S. minnesota*	TLR4 (10)
Flagellin	*S. typhimurium*	TLR5 (9)
PGN	*S. aureus*	TLR2 (8)
Pam_3CSK_4	Synthesis (*E. coli*) (16)	TLR1/TLR2 (41)
FSL-1	Synthesis (*M. salivarium*) (18)	TLR2/TLR6 (17)
MALP-2	Synthesis (*M. fermentans*) (19)	TLR2/TLR6 (55)

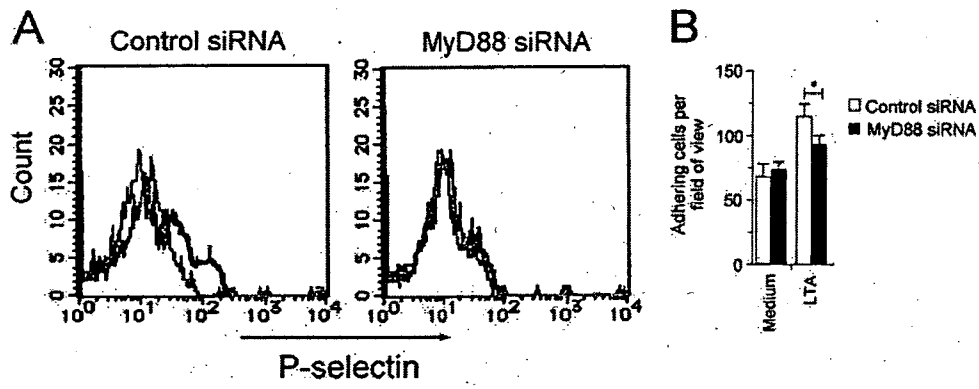

FIGURE 2. **MyD88-dependent P-selectin externalization by LTA.** *A*, HAECs transfected with MyD88-specific or control siRNA were stimulated with 10 μg/ml LTA for 60 min, and then surface P-selectin was detected by flow cytometry. *Shaded histogram*, not stimulated; *gray*, stimulated with LTA. *B*, HAECs transfected with MyD88-specific or control siRNA were stimulated with 10 μg/ml LTA for 60 min, and monocytes stained with conA-Alexa594 were then allowed to adhere for 20 min. Adhesion of red fluorescent cells was quantified in three fields per well by using an image analysis system. Each value is the mean ± S.D. ($n = 3$). *, $p < 0.01$.

Regarding the process of Weibel-Palade body exocytosis, we found that MyD88-dependent externalization of P-selectin was induced after stimulation of HAECs with LTA for 30 min (Fig. 2*A*). In addition, monocyte adhesion to HAECs was modestly increased in a MyD88-dependent fashion after LTA stimulation for 60 min (Fig. 2*B*).

Stimulatory Activities of LPS and PGN in HAECs—As stated above, LPS did not activate Weibel-Palade body exocytosis (Fig. 1*D*). However, LPS potently activated induction of MyD88-dependent IL-8 production in HAECs after stimulation for 4 h (Fig. 3*A*). Thus, the results shown in Figs. 1*D* and 3*A* suggest that endothelial TLR4 lacks the ability to induce rapid Weibel-Palade body exocytosis without *de novo* protein synthesis. Similarly to LPS, PGN did not activate Weibel-Palade body exocytosis (Fig. 1*D*). Also, PGN did not induce IL-8 production after stimulation for 4 h in HAECs, whereas LTA did (Fig. 3*A*). However, our preparation of PGN had activities to induce TNF-α production in THP-1 monocytes (Fig. 3*B*) and TLR2- and MyD88-dependent activation of NF-κB in HEK293 cells (Fig. 3*C*) in a way similar to that in the case of other TLR2 agonists. These results suggest that HAECs lack the ability to respond to PGN.

Induction of Weibel-Palade Body Exocytosis through TLR2—We then focused on LTA- and bacterial lipopeptide-induced Weibel-Palade body exocytosis. It has been reported that LTA and bacterial lipopeptides are TLR2 agonists (Table 1). In HUVECs, the lipopeptide FSL-1 induced VWF release (Fig. 4*A*). We found that this response was enhanced by increased expression of TLR2 by gene transfection (Fig. 4*A*). This result suggests that TLR2 recognition of bacterial constituents directly activates Weibel-Palade body exocytosis. Moreover, transfection of mutated TLR2 (P681H), which lacks the ability to interact with MyD88 (26), suppressed the release (Fig. 4*B*), consistent with the results presented in Figs. 1*D* and 2*A* showing that MyD88 was involved in the induction of Weibel-Palade exocytosis. In HAECs, knockdown of TLR2 expression resulted in almost complete suppression of VWF release by Pam_3CSK_4, FSL-1, MALP-2, and LTA (Fig. 4*B*). Moreover, knockdown of TLR6 expression resulted in a decrease in the activities of LTA, FSL-1, and MALP-2 and even that of Pam_3CSK_4 (Fig. 4*B*). In contrast to this, TLR1 interference did not affect VWF release (Fig. 4*B*), consistent with our observation that HAECs express very low levels of TLR1 mRNA compared with the levels of TLR2 mRNA (data not shown). These results suggest that endothelial recognition of pathogens by TLR2, or to a lesser extent by TLR6, contributes to induction of Weibel-Palade body exocytosis.

Involvement of PLCγ Activation in Weibel-Palade Body Exocytosis—Recent studies have shown that TLR2 signal transduction results in an increase of intracellular calcium level (27, 28). Indeed, we found that the intracellular calcium chelator BAPTA-AM suppressed LTA-induced exocytosis (Fig. 5*A*). We

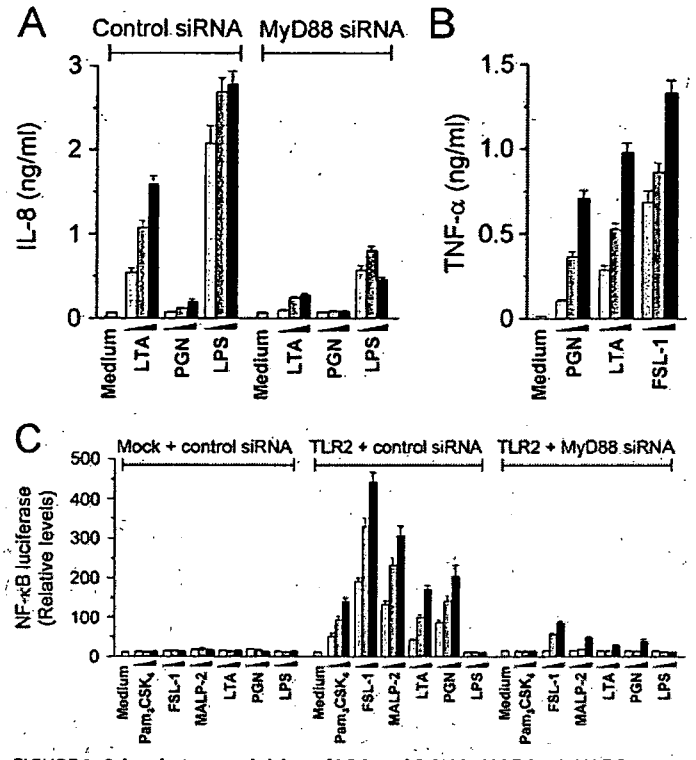

FIGURE 3. **Stimulatory activities of LPS and PGN in HAECs.** *A*, HAECs transfected with MyD88-specific or control siRNA were stimulated with LTA (0.1–10 μg/ml), PGN (0.1–10 μg/ml), and LPS (1–100 ng/ml) for 4 h, and then the amounts of IL-8 released into the media were measured. Each value is the mean ± S.D. ($n = 3$). *B*, THP-1 cells were stimulated with PGN (0.1–10 μg/ml), LTA (0.1–10 μg/ml), and FSL-1 (10–1 μg/ml) for 6 h, and then the amounts of TNF-α released into the media were measured. Each value is the mean ± S.D. ($n = 3$). *C*, HEK293 cells stably expressing TLR2, and control cells were prepared and then transfected with MyD88-specific siRNA and NF-κB-driven luciferase gene. The cells were stimulated with Pam_3CSK_4 (0.1–10 μg/ml), FSL-1 (0.01–1 μg/ml), MALP-2 (0.01–1 μg/ml), LTA (0.1–10 μg/ml), PGN (0.1–10 μg/ml), and LPS (1–100 ng/ml) for 6 h, and then luciferase activity was measured. Each value is the mean ± S.D. ($n = 3$).

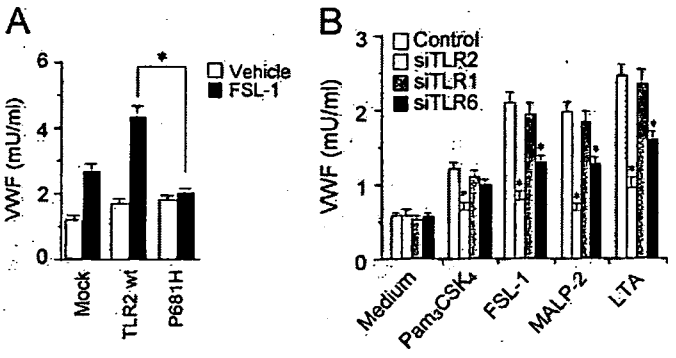

FIGURE 4. **Involvement of TLR2 in Weibel-Palade body exocytosis.** *A*, HUVECs transfected with WT or P681H mutant of TLR2 or with a control plasmid were stimulated with 1 μg/ml FSL-1 for 60 min, and then the amounts of VWF released into the media were measured. Each value is the mean ± S.D. ($n = 3$). *B*, HAECs transfected with TLR1-, TLR2-, or TLR6-specific or control siRNA were stimulated with Pam_3CSK_4 (10 μg/ml), FSL-1 (1 μg/ml), MALP-2 (1 μg/ml), and LTA (10 μg/ml) for 60 min, and then the amounts of VWF released into the media were measured. Each value is the mean ± S.D. ($n = 3$). *, $p < 0.05$.

therefore examined the role of PLCγ, a common regulator of intracellular calcium release by generating inositol 1,4,5-triphosphate (29), during TLR2-mediated Weibel-Palade body exocytosis. We found that the PLCγ inhibitor U-73122 significantly suppressed TLR2 agonist-induced VWF release (Fig. 5*B*). Because PLCγ isoforms are thought to be activated by phosphatidylinositol 3,4,5-trisphosphate, the product of phosphatidylinositol 3-kinases (PI3Ks) (29), TLR2-mediated exocytosis was suppressed by the chemical inhibitor of PI3K LY294002 (data not shown). However, downstream of TLR/IL-1R, activation of PI3K is regulated through a MyD88-independent machinery (30), conflicting with our results showing that Weibel-Palade body exocytosis requires MyD88 (Figs. 1*D* and 2*A*). Because enzymatic activity of PLCγ is also regulated by tyrosine phosphorylation (31), we tested whether this event was mediated by MyD88. Phosphorylation of PLCγ1 at the Tyr-738 residue was induced by LTA stimulation (Fig. 5*C*). Interestingly, this activity was efficiently suppressed by knockdown of MyD88 expression but not by knockdown of IRAK-1 expression (Fig. 5*C*). MyD88-dependent activation of PLCγ was also observed in TLR2-overexpressed 293 cells used as non-endothelial cells (data not shown). These results suggest that TLR2-mediated rapid Weibel-Palade body exocytosis is regulated by activation of PLCγ through MyD88-dependent tyrosine phosphorylation.

We also investigated the role of PLCγ in TLR2-mediated NF-κB signaling. U-73122 treatment clearly suppressed TLR2 agonist-induced production of the NF-κB-driven chemokine IL-8 in HAECs (Fig. 5*D*). U-73122 treatment also suppressed LTA-induced phosphorylation and degradation of IκBα in HAECs (Fig. 5*E*). These results suggest that the MyD88-PLCγ pathway also mediates inflammatory responses through NF-κB activation in endothelial cells.

Regulation of TLR2-mediated Weibel-Palade Body Exocytosis—The results shown in Fig. 4 (*A* and *B*) raised the possibility that alteration of endothelial TLR2 expression affects the magnitude of Weibel-Palade body exocytosis. We examined TLR2-mediated exocytosis in the presence of vascular modulators, IFN-γ or laminar flow, which are known to affect TLR2 expression in endothelial cells of human origin. Consistent with the results of a previous study (32), treatment with IFN-γ increased TLR2 expression level in HAECs (Fig. 6*A*). Under this condition, the magnitude of TLR2-mediated exocytosis was significantly increased (Fig. 6*B*). In contrast to this, TLR2 expression slightly decreased in HAECs incubated under laminar flow (Fig. 6*C*), consistent with the results of a previous study (33). We found that laminar flow decreased the magnitude of TLR2-mediated exocytosis (Fig. 6*D*).

DISCUSSION

The major finding of this study is that aortic endothelial cells respond to several bacterial constituents that stimulate TLR2, leading to induction of Weibel-Palade body exocytosis through a MyD88-dependent mechanism without *de novo* protein synthesis. During this process, release of VWF and externalization of P-selectin were induced, by which rolling and adhesion of platelets and leukocytes and thrombus formation in the local vessel walls may be promoted (34, 35). The pathological role of this phenomenon *in vivo* may be support by the observations in mouse experiments, *i.e.* slight increases of local leukocyte-endothelial interaction after LTA administration (36) and soluble P-selectin level in serum after administration of the synthetic

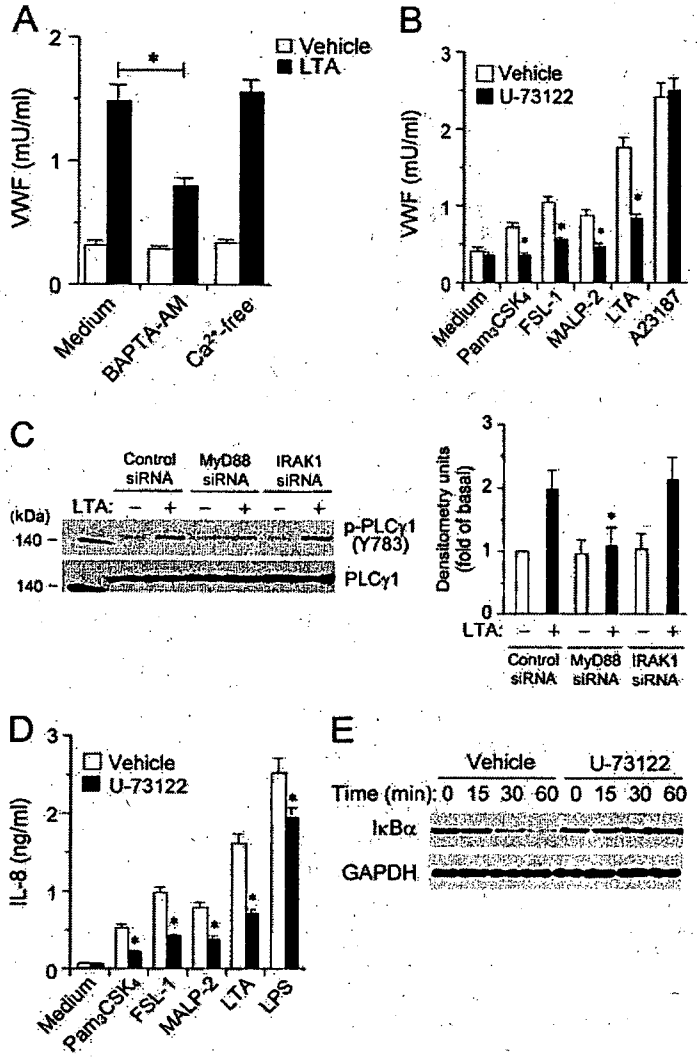

FIGURE 5. **PLCγ-mediation of TLR2-activated Weibel-Palade body exocytosis and NF-κB activation.** *A*, confluent HAECs were pretreated with 20 μM BAPTA-AM for 30 min or incubated in Ca^{2+}-free media. Then the cells were washed and stimulated with 10 μg/ml LTA for 60 min in Ca^{2+}-free media. The amounts of VWF released into the media were measured by ELISA. Each value is the mean ± S.D. ($n = 3$). *, $p < 0.01$. *B*, HAECs were pretreated with 10 μM U-73122 for 30 min and then washed and stimulated with Pam_3CSK_4 (10 μg/ml), FSL-1 (1 μg/ml), MALP-2 (1 μg/ml), LTA (10 μg/ml), and A23187 (1 μM) for 60 min. The amounts of VWF released into the media were measured by ELISA. Each value is the mean ± S.D. ($n = 3$). *, *versus* vehicle group, $p < 0.01$. *C*, HAECs transfected with MyD88- or IRAK1-specific or control siRNA were stimulated with 10 μg/ml LTA for 90 min. Immunoblot analysis was then performed to examine the expression of phosphorylated PLCγ1 (Y783) and total PLCγ1 (*left*). Immunoreactive bands were quantified by a densitometer (*right*). Results are expressed as means ± S.D. of three independent experiments. *, *versus* control group, $p < 0.01$. *D*, HAECs were pretreated with 10 μM U73122 for 30 min and then washed and stimulated with Pam_3CSK_4 (10 μg/ml), FSL-1 (1 μg/ml), MALP-2 (1 μg/ml), LTA (10 μg/ml), and A23187 (1 μM) for 4 h. The amounts of IL-8 released into the media were measured by ELISA. Each value is the mean ± S.D. ($n = 3$). *, *versus* vehicle group, $p < 0.01$. *E*, HAECs were pretreated with 10 μM U73122 for 30 min and then washed and stimulated with 10 μg/ml LTA for the indicated period. Immunoblot analysis was then performed to examine the expression of IκBα and glyceraldehyde-3-phosphate dehydrogenase (*GAPDH*).

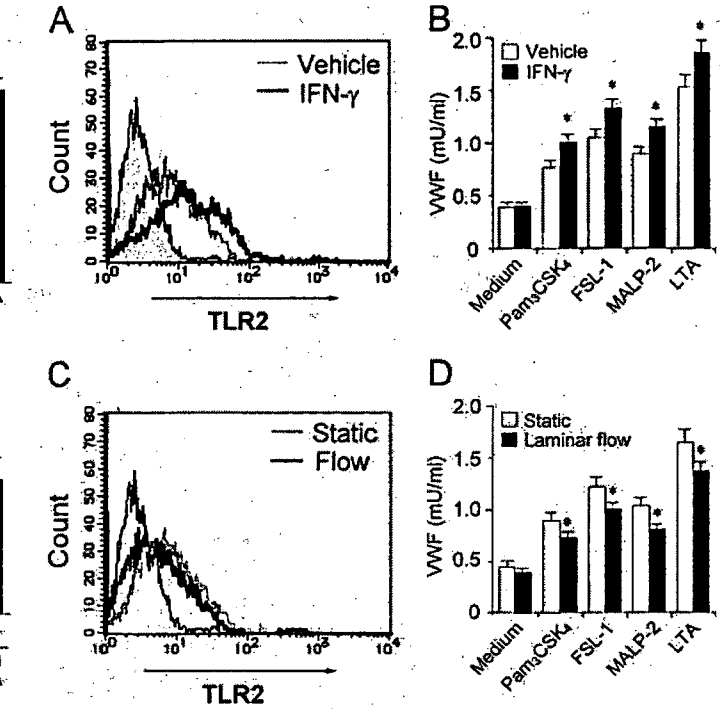

FIGURE 6. **Regulation of TLR2-mediated Weibel-Palade body exocytosis.** *A* and *B*, HAECs were treated with IFN-γ for 12 h. Surface TLR2 expression was detected by flow cytometry (*A*). The *shaded histogram* indicates cells stained with control antibody. The cells were washed and stimulated with Pam_3CSK_4 (10 μg/ml), FSL-1 (1 μg/ml), MALP-2 (1 μg/ml), and LTA (10 μg/ml) for 60 min. The amounts of VWF released into the media were measured by ELISA (*B*). Each value is the mean ± S.D. ($n = 3$). *, *versus* vehicle group, $p < 0.05$. *C* and *D*, HAECs were incubated under laminar flow for 12 h. Surface TLR2 expression was detected by flow cytometry (*C*). The *shaded histogram* indicates cells stained with control antibody. The cells were then stimulated with Pam_3CSK_4 (10 μg/ml), FSL-1 (1 μg/ml), MALP-2 (1 μg/ml), and LTA (10 μg/ml) for 60 min. The amounts of VWF released into the media were measured by ELISA (*D*). Each value is the mean ± S.D. ($n = 3$). *, *versus* static group, $p < 0.05$.

lipopeptide FSL-1.[3] Sequentially or simultaneously, both PLCγ- and IRAK1-mediated signaling pathways activate NF-κB, by which production of various proinflammatory cytokines, and expression of adhesion molecules such as ICAM-1 are induced to promote adherence and activation of platelets and leukocytes (37). The delayed Weibel-Palade body exocytosis with *de novo* protein synthesis is further activated in the cells. Therefore, endothelial TLR2 may be able to function as a primary initiator and a modulator of artery inflammation through these early-phase endothelial responses after recognition of cognate agonists.

We investigated the responsiveness of HAECs toward common bacterial constituents. For the TLR2 agonists, we prepared several compounds that have already been proposed to function as TLR2 agonists, because TLR2 forms a complicated recognition system and because human endothelial cells from different vascular beds show different degrees of responsiveness to TLR2 agonists (32, 38, 39). Unexpectedly, PGN, unlike other TLR2 agonists, could not activate either Weibel-Palade body exocytosis or IL-8 production (Figs. 1*D* and 3*A*). The issue of recognition of PGN by TLR2 is still controversial. The existence of an intracellular receptor for PGN (NOD2) further complicates this matter. However, Gupta's group recently concluded that PGN is in fact recognized by TLR2 by showing that muramidase treatment of PGN abolished the TLR2-stimulating activity (8). We showed that recognition of our PGN was at least dependent on TLR2 (Fig. 3*A*). It has been shown that PGN directly binds TLR2 *per se* (40), whereas bacterial lipopeptides

[3] T. Into, Y. Kanno, J.-i. Dohkan, M. Nakashima, M. Inomata, K.-i. Shibata, C. J. Lowenstein, and K. Katsushita, unpublished data.

are thought to directly interact with TLR2-associated molecules such as CD14 and LBP but not with TLR2 *per se* (7, 41, 42), suggesting the existence of different ligand-recognition mechanisms by TLR2. Furthermore, a novel family of PGN-binding proteins such as peptidoglycan recognition proteins has been found (43) and might enable discrimination of PGN from other TLR2 agonists. Thus, PGN may be recognized by a TLR2 recognition system different from that for LTA and lipoproteins/lipopeptides. Collectively, HAECs express functional TLR2 to respond to several TLR2 agonists, including lipopeptides and LTA, but may lack a PGN-recognition system resulting in an inability to respond to PGN. Moreover, aortic endothelial cells may particularly recognize diacylglyceride-containing bacterial lipid derivatives (LTA and bacterial lipopeptides), recognition of which has recently been reported to depend on TLR6 and CD36 (11).

We also showed that the TLR4 agonist LPS did not activate Weibel-Palade body exocytosis (Fig. 1*D*). Although the reason for this is not clear, several lines of evidence obtained in previous studies may provide an explanation. For example, TLR4 expression has been reported to localize intracellularly in artery endothelial cells (44). This observation suggests that TLR4 in artery endothelial cells may be lacking in induction of phospholipid-dependent signaling events, including PLCγ activation, which are commonly intrinsic to the signaling receptors spanning the cell membrane. Further investigation is needed to determine the reason.

Several properties of endothelial TLR2 have been proposed to be involved in the development of atherosclerosis. First, endothelial TLR2 expression is enhanced by proinflammatory stimuli, such as TNF-α, IFN-γ, and LPS (32), and by SP-1-dependent machinery in areas of disturbed blood flow such as lesion predilection within the aortic tree and heart (33). The expression level of TLR2 is indeed increased in an atherosclerotic lesion in humans (45). Furthermore, a recent study has revealed that complete deficiency of TLR2 in atherosclerosis-prone LDLR-null mice leads to an apparent reduction in the formation of lesions (46). Proinflammatory signaling pathways downstream of TLR2 have been thought to be activated through TIRAP/Mal, MyD88, IRAK-1, and TRAF6 in endothelial cells. Other pathways involving PI3K and the downstream protein kinase Akt/PKB (47), the Rho family GTPase Rac1 (48), and the redox-activated mitogen-activated protein kinase kinase kinase ASK1 (49) also link TLR2 signaling to the NF-κB pathway. In this study, we showed that PLCγ also mediated the NF-κB pathway downstream of TLR2 in HAECs, although involvement of PLCγ in the TLR2 proinflammatory signaling has been described in several reports (27, 50). Because PLCγ isoforms are thought to be activated by both generation of phosphatidylinositol 3,4,5-triphosphate by PI3K and tyrosine phosphorylation, we found the latter process downstream of TLR2 was dependent on MyD88 but not IRAK-1 (Fig. 5*C*). Recent studies have suggested a linkage of TLRs and tyrosine kinases, including Syk via MyD88-STAP-2 interaction (51) and Btk via direct interaction with TIR domain (52), both of which have been shown to activate PLCγ isoforms. Moreover, Btk-induced phosphorylation of TIRAP/Mal has recently been reported to play an important role in TLR signal transduction

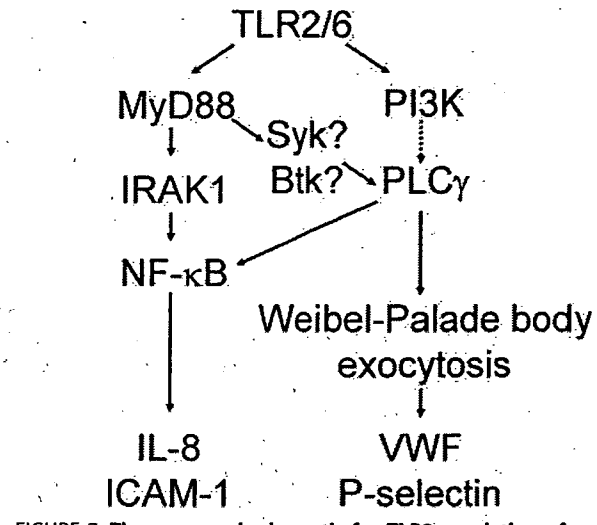

FIGURE 7. **The proposed schematic for TLR2 regulation of early-phase inflammatory signaling in human aortic endothelial cells.**

(53), which may occur at a phosphatidylinositol diphosphate-rich membrane compartment after recruitment of MyD88 to membrane-localized TIRAP/Mal (54). A schematic of signaling pathways proposed here is shown in Fig. 7.

Endothelial activation by several proinflammatory agents has been shown to increase endothelial responsiveness toward TLR2 agonists via up-regulation of TLR2 expression (32). Increased endothelial TLR2 expression increased the magnitude of TLR2-mediated exocytosis of Weibel-Palade bodies (Fig. 6*B*) and endothelial responses (38), suggesting enhanced responsiveness of endothelial cells to pathogens in inflamed lesions. In contrast, fluid shear decreased the magnitude of TLR2 ligand-stimulated Weibel-Palade body exocytosis (Fig. 6*D*). Physiological fluid shear stress has been suggested to have atheroprotective effects *in vivo*, because atherosclerosis preferentially occurs in an area of disturbed flow or a low level of shear stress, whereas regions with steady laminar flow and physiological shear stress are protected. Disturbed flow or a low level of shear stress has been reported to regulate expression of various regulatory molecules of endothelial activation, by which atherosclerotic processes may be accelerated in the sites. These observations are consistent with the previous finding that physiological fluid shear stress decreases endothelial TLR2 expression via impaired activity of the transcriptional factor SP1 (33). Thus, our results raise the possibility that bacterial constituent-induced Weibel-Palade body exocytosis can be physiologically or pathologically regulated in particular circumstances of the vessel wall.

In conclusion, our study focused on endothelial exocytosis induced by bacterial pathogens and showed a linkage between endothelial innate recognition of pathogens and early-phase endothelial inflammatory responses. Our results may provide a new insight into the role of endothelial TLR2 in the initiation and modulation of vascular inflammation or atherogenic responses.

REFERENCES

1. Lowenstein, C. J., Morrell, C. N., and Yamakuchi, M. (2005) *Trends Cardiovasc. Med.* **15**, 302–308
2. Rondaij, M. G., Bierings, R., Kragt, A., van Mourik, J. A., and Voorberg, J.

(2006) *Arterioscler. Thromb. Vasc. Biol.* **26,** 1002–1007
3. Danesh, J. (1999) *Am. Heart J.* **138,** S434–S437
4. Desvarieux, M., Demmer, R. T., Rundek, T., Boden-Albala, B., Jacobs, D. R., Jr., Sacco, R. L., and Papapanou, P. N. (2005) *Circulation* **111,** 576–582
5. Akira, S., and Takeda, K. (2004) *Nat. Rev. Immunol.* **4,** 499–511
6. Kirschning, C. J., and Schumann, R. R. (2002) *Curr. Top. Microbiol. Immunol.* **270,** 121–144
7. Schroder, N. W., Morath, S., Alexander, C., Hamann, L., Hartung, T., Zahringer, U., Gobel, U. B., Weber, J. R., and Schumann, R. R. (2003) *J. Biol. Chem.* **278,** 15587–15594
8. Dziarski, R., and Gupta, D. (2005) *Infect. Immun.* **73,** 5212–5216
9. Reed, K. A., Hobert, M. E., Kolenda, C. E., Sands, K. A., Rathman, M., O'Connor, M., Lyons, S., Gewirtz, A. T., Sansonetti, P. J., and Madara, J. L. (2002) *J. Biol. Chem.* **277,** 13346–13353
10. Tapping, R. I., Akashi, S., Miyake, K., Godowski, P. J., and Tobias, P. S. (2000) *J. Immunol.* **165,** 5780–5787
11. Hoebe, K., Georgel, P., Rutschmann, S., Du, X., Mudd, S., Crozat, K., Sovath, S., Shamel, L., Hartung, T., Zahringer, U., and Beutler, B. (2005) *Nature* **433,** 523–527
12. Jeannin, P., Bottazzi, B., Sironi, M., Doni, A., Rusnati, M., Presta, M., Maina, V., Magistrelli, G., Haeuw, J. F., Hoeffel, G., Thieblemont, N., Corvaia, N., Garlanda, C., Delneste, Y., and Mantovani, A. (2005) *Immunity* **22,** 551–560
13. Mullaly, S. C., and Kubes, P. (2004) *Circ. Res.* **95,** 657–659
14. Tobias, P., and Curtiss, L. K. (2005) *J. Lipid Res.* **46,** 404–411
15. Michelsen, K. S., Doherty, T. M., Shah, P. K., and Arditi, M. (2004) *J. Immunol.* **173,** 5901–5907
16. Hoffmann, P., Heinle, S., Schade, U. F., Loppnow, H., Ulmer, A. J., Flad, H. D., Jung, G., and Bessler, W. G. (1988) *Immunobiology* **177,** 158–170
17. Fujita, M., Into, T., Yasuda, M., Okusawa, T., Hamahira, S., Kuroki, Y., Eto, A., Nisizawa, T., Morita, M., and Shibata, K. (2003) *J. Immunol.* **171,** 3675–3683
18. Shibata, K., Hasebe, A., Into, T., Yamada, M., and Watanabe, T. (2000) *J. Immunol.* **165,** 6538–6544
19. Muhlradt, P. F., Kiess, M., Meyer, H., Sussmuth, R., and Jung, G. (1997) *J. Exp. Med.* **185,** 1951–1958
20. Into, T., Kiura, K., Yasuda, M., Kataoka, H., Inoue, N., Hasebe, A., Takeda, K., Akira, S., and Shibata, K. (2004) *Cell Microbiol.* **6,** 187–199
21. Matsushita, K., Morrell, C. N., Cambien, B., Yang, S. X., Yamakuchi, M., Bao, C., Hara, M. R., Quick, R. A., Cao, W., O'Rourke, B., Lowenstein, J. M., Pevsner, J., Wagner, D. D., and Lowenstein, C. J. (2003) *Cell* **115,** 139–150
22. Dimmeler, S., Haendeler, J., Rippmann, V., Nehls, M., and Zeiher, A. M. (1996) *FEBS Lett.* **399,** 71–74
23. Doran, K. S., Engelson, E. J., Khosravi, A., Maisey, H. C., Fedtke, I., Equils, O., Michelsen, K. S., Arditi, M., Peschel, A., and Nizet, V. (2005) *J. Clin. Invest.* **115,** 2499–2507
24. Bermpohl, D., Halle, A., Freyer, D., Dagand, E., Braun, J. S., Bechmann, I., Schroder, N. W., and Weber, J. R. (2005) *J. Clin. Invest.* **115,** 1607–1615
25. Talreja, J., Kabir, M. H., Filla, M. B., Stechschulte, D. J., and Dileepan, K. N. (2004) *Immunology* **113,** 224–233
26. Xu, Y., Tao, X., Shen, B., Horng, T., Medzhitov, R., Manley, J. L., and Tong, L. (2000) *Nature* **408,** 111–115
27. Chun, J., and Prince, A. (2006) *J. Immunol.* **177,** 1330–1337
28. Supajatura, V., Ushio, H., Nakao, A., Akira, S., Okumura, K., Ra, C., and Ogawa, H. (2002) *J. Clin. Invest.* **109,** 1351–1359
29. Bae, Y. S., Cantley, L. G., Chen, C. S., Kim, S. R., Kwon, K. S., and Rhee, S. G. (1998) *J. Biol. Chem.* **273,** 4465–4469
30. Davis, C. N., Mann, E., Behrens, M. M., Gaidarova, S., Rebek, M., Rebek, J., Jr., and Bartfai, T. (2006) *Proc. Natl. Acad. Sci. U. S. A.* **103,** 2953–2958
31. Law, C. L., Chandran, K. A., Sidorenko, S. P., and Clark, E. A. (1996) *Mol. Cell Biol.* **16,** 1305–1315
32. Faure, E., Thomas, L., Xu, H., Medvedev, A., Equils, O., and Arditi, M. (2001) *J. Immunol.* **166,** 2018–2024
33. Dunzendorfer, S., Lee, H. K., and Tobias, P. S. (2004) *Circ. Res.* **95,** 684–691
34. Andre, P., Denis, C. V., Ware, J., Saffaripour, S., Hynes, R. O., Ruggeri, Z. M., and Wagner, D. D. (2000) *Blood* **96,** 3322–3328
35. Massberg, S., Brand, K., Gruner, S., Page, S., Muller, E., Muller, I., Bergmeier, W., Richter, T., Lorenz, M., Konrad, I., Nieswandt, B., and Gawaz, M. (2002) *J. Exp. Med.* **196,** 887–896
36. Yipp, B. G., Andonegui, G., Howlett, C. J., Robbins, S. M., Hartung, T., Ho, M., and Kubes, P. (2002) *J. Immunol.* **168,** 4650–4658
37. Collins, T., Read, M. A., Neish, A. S., Whitley, M. Z., Thanos, D., and Maniatis, T. (1995) *FASEB J.* **9,** 899–909
38. Bulut, Y., Faure, E., Thomas, L., Equils, O., and Arditi, M. (2001) *J. Immunol.* **167,** 987–994
39. Faure, E., Equils, O., Sieling, P. A., Thomas, L., Zhang, F. X., Kirschning, C. J., Polentarutti, N., Muzio, M., and Arditi, M. (2000) *J. Biol. Chem.* **275,** 11058–11063
40. Iwaki, D., Mitsuzawa, H., Murakami, S., Sano, H., Konishi, M., Akino, T., and Kuroki, Y. (2002) *J. Biol. Chem.* **277,** 24315–24320
41. Manukyan, M., Triantafilou, K., Triantafilou, M., Mackie, A., Nilsen, N., Espevik, T., Wiesmuller, K. H., Ulmer, A. J., and Heine, H. (2005) *Eur. J. Immunol.* **35,** 911–921
42. Schroder, N. W., Heine, H., Alexander, C., Manukyan, M., Eckert, J., Hamann, L., Gobel, U. B., and Schumann, R. R. (2004) *J. Immunol.* **173,** 2683–2691
43. Dziarski, R., and Gupta, D. (2006) *Cell Microbiol.* **8,** 1059–1069
44. Dunzendorfer, S., Lee, H. K., Soldau, K., and Tobias, P. S. (2004) *FASEB J.* **18,** 1117–1119
45. Edfeldt, K., Swedenborg, J., Hansson, G. K., and Yan, Z. Q. (2002) *Circulation* **105,** 1158–1161
46. Mullick, A. E., Tobias, P. S., and Curtiss, L. K. (2005) *J. Clin. Invest.* **115,** 3149–3156
47. Martin, M., Schifferle, R. E., Cuesta, N., Vogel, S. N., Katz, J., and Michalek, S. M. (2003) *J. Immunol.* **171,** 717–725
48. Arbibe, L., Mira, J. P., Teusch, N., Kline, L., Guha, M., Mackman, N., Godowski, P. J., Ulevitch, R. J., and Knaus, U. G. (2000) *Nat. Immunol.* **1,** 533–540
49. Into, T., and Shibata, K. (2005) *Cell Microbiol.* **7,** 1305–1317
50. Lee, C. W., Chien, C. S., and Yang, C. M. (2004) *Am. J. Physiol.* **286,** L921–L930
51. Sekine, Y., Yumioka, T., Yamamoto, T., Muromoto, R., Imoto, S., Sugiyma, K., Oritani, K., Shimoda, K., Minoguchi, M., Akira, S., Yoshimura, A., and Matsuda, T. (2006) *J. Immunol.* **176,** 380–389
52. Horwood, N. J., Page, T. H., McDaid, J. P., Palmer, C. D., Campbell, J., Mahon, T., Brennan, F. M., Webster, D., and Foxwell, B. M. (2006) *J. Immunol.* **176,** 3635–3641
53. Gray, P., Dunne, A., Brikos, C., Jefferies, C. A., Doyle, S. L., and O'Neill, L. A. (2006) *J. Biol. Chem.* **281,** 10489–10495
54. Kagan, J. C., and Medzhitov, R. (2006) *Cell* **125,** 943–955
55. Nakao, Y., Funami, K., Kikkawa, S., Taniguchi, M., Nishiguchi, M., Fukumori, Y., Seya, T., and Matsumoto, M. (2005) *J. Immunol.* **174,** 1566–1573

Biochem. J. (2007) 405, 69–75 (Printed in Great Britain) doi:10.1042/BJ20070104

Runx3 negatively regulates Osterix expression in dental pulp cells

Li ZHENG*, Koichiro IOHARA*, Masaki ISHIKAWA†, Takeshi INTO*, Teruko TAKANO-YAMAMOTO‡, Kenji MATSUSHITA* and Misako NAKASHIMA*[1]

*Laboratory of Oral Disease Research, National Institute for Longevity Sciences, National Center for Geriatrics and Gerontology, Aichi 474-8522, Japan, †Department of Endodontology and Operative Dentistry, Division of Oral Rehabilitation, Faculty of Dental Science, Kyushu University, Fukuoka 812-8582, Japan, and ‡Division of Orthodontics and Dentofacial Orthopedics, Graduate School of Dentistry, Tohoku University, Sendai 980-8575, Japan

Osterix, a zinc-finger-containing transcription factor, is required for osteoblast differentiation and bone formation. *Osterix* is also expressed in dental mesenchymal cells of the tooth germ. However, transcriptional regulation by Osterix in tooth development is not clear. Genetic studies in osteogenesis place *Osterix* downstream of Runx2 (Runt-related 2). The expression of *Osterix* in odontoblasts overlaps with Runx3 during terminal differentiation *in vivo*. Runx3 down-regulates *Osterix* expression in mouse DPCs (dental pulp cells). Therefore the regulatory role of Runx3 on *Osterix* expression in tooth development was investigated. Enforced expression of Runx3 down-regulated the activity of the *Osterix* promoter in the human embryonic kidney 293 cell line. When the Runx3 responsive element on the *Osterix* promoter, located at −713 to −707 bp (site 3, AGTGGTT) relative to the cap site, was mutated, this down-regulation was abrogated. Furthermore, electrophoretic mobility-shift assay and chromatin immunoprecipitation assays in mouse DPCs demonstrated direct functional binding of Runx3 to the *Osterix* promoter. These results demonstrate the transcriptional regulation of *Osterix* expression by Runx3 during differentiation of dental pulp cells into odontoblasts during tooth development.

Key words: bone morphogenetic protein 2 (BMP2), dental pulp cell (DPC), Osterix, Runx2, Runx3, tooth development.

INTRODUCTION

The transcriptional regulation of cell proliferation and differentiation by the Runx (Runt-related) family of DNA-binding transcription factors is critical for both morphogenesis and regeneration. The regulatory function of the Runx family on the promoters and enhancers of target genes, where they associate with cofactors and other DNA-binding transcription factors to modulate gene expression, is well known [1]. The Runx family is composed of three members designated Runx1 (AML1/Cbfα2), Runx2 (AML2/Cbfα1) and Runx3 (AML3/Cbfα3) [2,3]. Although the Runx members share highly conserved DNA-binding domains, they regulate distinct functions [4–7]. Runx1 is involved in the regulation of haematopoiesis [8], Runx2 is essential for bone and tooth development [9–11], and Runx3 is critical for gastric epithelial differentiation, neurogenesis of the dorsal root ganglia and T cell differentiation [8–10,12–16].

Stringent control of gene activation and suppression is required for tooth development. The optimal gene expression during dentin formation is dependent on integration and regulation of signals that govern the commitment of stem/progenitor cells into the pulp cell lineage, and their subsequent proliferation and differentiation into odontoblasts. Runx2 is essential for tooth formation. Molar development is arrested at the late bud stage in Runx2 homozygous mice [11], correlating with the intense expression of Runx2 in the dental mesenchyme during the bud and cap stages [17]. Runx3 is co-expressed in dental papillae at the cap and early bell stages, along with Runx2. Later Runx3 is restricted to the odontoblastic layer at the late bell stage, while Runx2 is no longer detected [17]. Runx proteins might play a pivotal role in governing the control of the physiological response of dental genes.

Osterix, a zinc-finger-containing transcription factor, is required for osteoblast differentiation and bone formation [18]. In *Osterix* null mice, no bone formation occurs, similar to the phenotypes in *Runx2* null mice [9,18]. However, Runx2 is expressed without major alterations in *Osterix* null mice. In contrast, Osterix is not expressed in *Runx2* null mice, demonstrating that Osterix acts downstream of Runx2 [18]. Transcriptional regulation of *Osterix* by Runx2 in cartilage has been suggested recently [19]. In addition, *Osterix* expression has been observed in mesenchymal cells of the tooth germ [18]. The expression of *Osterix* and its transcriptional regulation by Runx proteins during tooth development have not been investigated.

In the present study, we investigated the expression of *Osterix* during tooth development, and demonstrate that *Osterix* is expressed strictly in the odontoblastic layer at the bell and the differentiation stages, overlapping with *Runx3*. Therefore the regulation of the expression of *Osterix* by Runx3 was examined further. Our results demonstrate that Runx3 binds directly to the *Osterix* promoter and down-regulates its expression in DPCs (dental pulp cells).

EXPERIMENTAL

Cloning of the *Osterix* promoter

To clone the Osterix promoter (nucleotides 66 to 1751; GenBank accession no. DQ229136), genomic DNA was isolated from the tail of an ICR mouse. PCR was performed using two primers: Osterix promoter 5′-1, 5′-TCTGTCCCTCAGTCCTGCTT-3′ and Osterix promoter 3′-2, 5-GGGCAAGTTGTCAGAGCTTC-3′. The approx. 1.7 kbp PCR product was then subcloned into MluI

Abbreviations used: BMP, bone morphogenetic protein; ChIP, chromatin immunoprecipitation; DIG, digoxigenin; DMEM, Dulbecco's modified Eagle's medium; DPC, dental pulp cell; Dspp, dentin sialophosphoprotein; DTT, dithiothreitol; EGFP, enhanced green fluorescent protein; EMSA, electrophoretic mobility-shift assay; FBS, foetal bovine serum; HEK-293, human embryonic kidney 293; KLK4, kallikrein 4; MSCV, murine stem cell virus; P1, postnatal day 1; RT, reverse transcription; Runx, Runt-related.

[1] To whom correspondence should be addressed (email misako@nils.go.jp).

and XhoI digested pGL3-promoter vector (Promega, Madison, WI, U.S.A.), and named pOsx1.7-luc. To prepare the MSCV (murine stem cell virus)-EGFP (enhanced green fluorescent protein)-FLAG-Runx3 expression vector, the following primers were used: FLAG-Runx3-5′, 5′-GGCAGATCTGCCACCATGGACTACAAGGACGATGACGACAAGGCTTCCAACAGCATCTTTG-3′ and Flag-Runx3-3′, 5′-ATATGAGCTCTCCCGCGTGGT-3′ to generate a Runx3 fragment with FLAG motif at N-terminal. The 300 bp PCR product was cloned in between the BglII and SacI sites in the pSL1180 vector (GE Healthcare, Buckinghamshire, U.K.) and named Flag-Runx3-300 bp-pSL1180. A 1.0 kbp Runx3 fragment was digested with SacI from the MSCV-EGFP-Runx3 plasmid (kindly provided by Dr Taniuchi Ichiro, Laboratory of Transcriptional Regulation, RIKEN Research Centre for Allergy and Immunology, Yokohama, Japan) and subcloned into the FLAG-Runx3-300 bp-pSL1180 vector to give FLAG-Runx3-pSL1180. The N-terminally FLAG-tagged full-length 1.3 kbp Runx3 was digested with BglII from FLAG-Runx3-pSL1180 and subcloned into the MSCV-EGFP vector, named MSCV-EGFP-FLAG-Runx3. The orientation of the inserts was confirmed by sequencing.

Site-directed mutagenesis

Three putative Runx2-binding sequences at positions −1823 to −1817 bp, −1776 to −1771 bp and −713 to −707 bp relative to the Cap site [19] were mutated using the QuikChange® Site-Directed Mutagenesis Kit (Stratagene, La Jolla, CA, U.S.A.) according to the manufacturer's recommendations. We generated mutants as follows; 5′-AACCACA-3′ at −1823/−1817 bp was changed into 5′-**GAGCTCA**-3′, 5′-ACCACT-3′ at −1776/−1771 bp was changed into 5′-**GCTACT**-3′ and 5′-AGTGGTT-3′ at −713/−707 bp was changed into 5′-A**TAGACT**-3′. The mutated nucleotides are indicated in bold. Mutations in single, double, and triple motifs were termed M1-M5 (Figure 3B). Incorporation of the mutated substitutions of all the constructs was confirmed by sequencing.

In situ hybridization

ICR mouse embryos at 15.0 days post coitum, 17.0 days post coitum and P1 (postnatal day 1) were fixed in 4% (w/v) paraformaldehyde at 4 °C overnight. *In situ* hybridization was carried out as described previously [20]. The following primers were used to amplify the mouse *Osterix* cDNA: Osterix-5′-1, 5′-GGTCCAGGCAACACACCTAC-3′ and Osterix-3′-2, 5′-GGTAGGGAGCTGGGTTAAGG-3′. The PCR product was ligated into the pBluescript II SK (−) vector (Stratagene). Mouse *Runx3* cDNA was removed from the MSCV-EGFP-Runx3 plasmid by digestion with EcoRI and then subcloned into the pBluescript II SK (−) vector. All inserts were confirmed by sequencing. The following cDNAs were used to generate sense (see Supplementary Figure 1 at http://www.BiochemJ.org/bj/405/bj4050069add.htm) and antisense riboprobes using either T3 or T7 RNA polymerase: a 184 bp murine Osterix fragment, a 1.2 kb Runx3 fragment and a 1.2 kb Bmp2 fragment. *In situ* hybridization was performed as described previously [21].

Cell culture and transfection studies

Mouse DPCs were isolated from tooth germ at 17.0 days post coitum. Mouse DPCs and HEK-293 (human embryonic kidney 293) cells were maintained in DMEM (Dulbecco's modified Eagle's medium) (Sigma, St. Louis, MO, U.S.A.) supplemented with 100 units/ml penicillin G, 100 μg/ml streptomycin (Invitrogen, Carlsbad, CA, U.S.A.) and 10% (v/v) FBS (foetal bovine serum; SAFC Biosciences, Lenexa, KS, U.S.A.). Experiments assessing promoter activity by luciferase reporter gene expression were performed as follows. HEK-293 cells (1×10^5) were plated in 24-well plates in serum-free DMEM without antibiotics 1 day before use, and transiently transfected with 2 μg of the promoter–luciferase reporter gene plasmids, 3 μg of expression plasmid and 0.2 μg of SV40 (simian virus 40) promoter construct (Promega) as an internal standardized control for transfection efficiency. Transfections were performed using 2 μl/well of Lipofectamine™ 2000 (Invitrogen) following the manufacturer's instructions. The MSCV-EGFP plasmid was also transfected as a control. After 4 h, the medium was replaced with DMEM supplemented with 10% (v/v) FBS and cultured for an additional 44 h. Cells were then lysed, and luciferase activity was determined using a Dual Luciferase Reporter Assay kit as instructed by the manufacturer (Promega). All activities were normalized against the co-transfected internal control plasmid pRL-SV40 (Promega). For overexpression experiments, 4×10^6 DPCs were transfected with 8 μg of expression plasmid using an ECM 830 Electroporator (BTX, San Diego, CA, U.S.A.) following the manufacturer's instructions, then plated on to a collagen type I-coated 35-mm-diameter dish (Iwaki, Chiba, Japan). After 4 h, the medium was replaced with DMEM and 10% (v/v) FBS. Cells were harvested at 0, 24 and 48 h after transfection. The cell viability was determined with Trypan Blue soon after transfection, and the efficiency was estimated by fluorescent microscopy 24 h after transfection with the plasmid vector AFP (kindly provided by Dr Hidesato Ogawa, Graduate School of Biological Sciences, Nara Institute of Science and Technology, Japan).

Table 1 Primers for RT-PCR

Name	Direction	Sequence	Product size (bp)	Accession number
β-Actin	Forward	5′-AAATCGTGCGTGACATCAAA-3′		
	Reverse	5′-AAGGAAGGCTGGAAAAGAGC-3′	178	X03765
Runx3	Forward	5′-GGTTCAACGACCTTCGATTC-3′		
	Reverse	5′-AGGCCTTGGTCTGGTCTTCT-3′	180	NM_019732
Runx2	Forward	5′-CAGACCAGCAGCACTCCATA-3′		
	Reverse	5′-CAGCGTCAACACCATCATTC-3′	178	NM_009820
Osterix	Forward	5′-GGTCCAGGCAACACACCTAC-3′		
	Reverse	5′-GGTAGGGAGCTGGGTTAAGG-3′	178	AF184902
Dspp	Forward	5′-GGAACTGCAGCACAGAATGA-3′		
	Reverse	5′-CAGTGTTCCCCTGTTCGTTT-3′	199	NM_010080
Enamelysin	Forward	5′-CGACAATGCTGAGAAGTGGA-3′		
	Reverse	5′-CCCTTTCACATCATCCTTGG-3′	180	NM_013903
Klk4	Forward	5′-TTGCAAACGATCTCATGCTC-3′		
	Reverse	5′-TGAGGTGGTACACAGGGTCA-3′	228	NM_019928

Real time RT (reverse transcriptase)-PCR analysis

Total RNA was extracted by using Trizol (Invitrogen), and 2 μg of freshly isolated RNA was reverse transcribed with SuperScript II RT (Invitrogen) following the manufacturer's recommendations. The resulting cDNA was then amplified by real time RT-PCR with a Light Cycler-FastStart DNA master SYBR Green I (Roche Diagnostics, Mannheim, Germany). The primers used in the RT-PCR analysis are presented in Table 1.

Preparation of nuclear extracts

Nuclear extract was isolated as described previously [22]. Briefly, mouse DPCs were washed with 10 ml of PBS, scraped into 1.5 ml of ice-cold PBS, and centrifuged at 100 *g* for 5 min. The pellet was suspended in 1 ml of PBS and centrifuged again at 660 *g*

for 15 s. After resuspension in cold buffer A [10 mM Hepes, pH 7.9, 10 mM KCl, 0.1 mM EDTA, 0.1 mM EGTA, 1mM DTT (dithiothreitol) and 0.5 mM PMSF] on ice for 15 min, the cell membranes were lysed by 0.5 % Nonidet P40 and then centrifuged at 660 *g* for 30 s. The pelleted nuclei were resuspended in cold buffer C (20 mM Hepes, pH 7.9, 0.4 M NaCl, 1mM EDTA, 1 mM EGTA, 1 mM DTT and 1 mM PMSF). The nuclear protein was extracted by shaking at 4 °C for 15 min, followed by centrifugation at 15000 *g* for 5 min and the supernatant fractions were collected. The protein content of the nuclear extracts was determined using the Bradford method [23].

EMSA (electrophoretic mobility-shift assay)

Individual oligonucleotides were annealed to equimolar amounts of their complementary strands (wild-type, Osterix-gel-WT-5′-1: 5′-CAGATCTCTAATTAGTGGTTTGGGGTTTGTTCCT-TTTC-3′ and Osterix-gel-WT-3′-2: 5′-GAAAAGGAACAAAC-CCCAAACCACTAATTAGAGATCTG-3′; mutant, Osterix-gel-MT-5′-1: 5′-CAGATCTCTAATTATAGACTTGGGGTTTGTTC-CTTTTC-3′ and Osterix-gel-MT-3′-2: 5′-GAAAAGGAACAA-ACCCCAAGTCTATAATTAGAGATCTG-3′) by heating to 95 °C for 5 min and cooling slowly to room temperature (25 °C). DIG (digoxigenin) Gel Shift Kit, 2nd generation (Roche Diagnostics) was used in the EMSA according to the manufacturer's protocol. Briefly, wild-type double-stranded oligonucleotide probes were labelled with DIG-11-ddUTP at the 3′-ends. The labelled probes (20 fmol) were added to 10 μg of nuclear extract in a binding buffer [20 mM Hepes, pH 7.6, 1 mM EDTA, 10 mM $(NH_4)_2SO_4$, 1 mM DTT, 0.2 % (w/v) Tween 20, 30 mM KCl, 25 ng/μl poly(dI-dC) · (dI-dC), 25 ng/μl poly(dA-dT) · (dA-dT) and 50 ng/μl poly L-lysine] at room temperature for 30 min. For competition experiments, 125-fold unlabelled oligonucleotides were added to the mixture. After incubation, the protein–DNA complexes were separated by native PAGE (6 % gels), transferred on to a nylon membrane (Whatman, New Jersey, NJ, U.S.A.) by contact-blotting, and detected by the DIG-detection kit. An anti-Runx3 antibody (Active Motif, Carlsbad, CA, U.S.A.) was used to examine the specificity of the protein–DNA complexes.

ChIP (chromatin immunoprecipitation) assay

Mouse DPCs were treated for 10 min with 1 % formaldehyde and washed three times with ice-cold PBS. The cells were harvested and centrifuged at 100 *g* for 5 min. The pellet was suspended in 200 μl of SDS lysis buffer [50 mM Tris/HCl, pH 8.0, 10 mM EDTA, 1 % (w/v) SDS, 1 mM PMSF, 1 μg/ml aprotinin and 1 μg/ml leupeptin] and incubated on ice for 20 min. The sample was sonicated for 7.5 min (high power, on 30 s, off 1 min) using a Bioruptor (Cosmo Bio, Tokyo, Japan) to produce soluble chromatin with an average size of 500 bp. The chromatin sample was then diluted 9-fold in ice-cold ChIP dilution buffer [50 mM Tris/HCl, pH 8.0, 167 mM NaCl, 1.1 % (v/v) Triton X-100, 0.11 % sodium deoxycholate, 1 mM PMSF, 1 μg/ml aprotinin and 1 μg/ml leupeptin]. From the diluted sample, 200 μl was removed as the input fraction and kept at 4 °C. The rest of the sample was pre-cleared for 6 h at 4 °C by incubation with 60 μl of protein G–Sepharose beads pre-blocked with salmon sperm DNA. The beads were removed by centrifugation at 10000 *g* for 10 s and the supernatant was collected. Rabbit anti-Runx3 polyclonal antibody (20 μg; Active Motif, Carlsbad, CA, U.S.A.) or 10 μg of goat anti-mouse Runx2 polyclonal antibody (Santa Cruz, CA, U.S.A.) was added and incubated overnight at 4 °C. To collect the immunocomplex, 60 μl of protein G–Sepharose beads pre-blocked with salmon sperm DNA were added to the samples for 3 h at 4 °C. The beads were washed once in each of the following buffers, in order: low salt, high salt and LiCl wash solution, and were then washed twice in TE buffer. The bound protein–DNA immunocomplexes were eluted twice with 200 μl of ChIP direct elution buffer (10 mM Tris/HCl, pH 8.0, 300 mM NaCl, 5 mM EDTA and 0.5 % SDS) and subjected to reverse cross-linking at 65 °C for 6 h. The reverse cross-linked chromatin DNA was further purified by 50 μg/ml proteinase K digestion at 55 °C for 1 h and phenol/chloroform extraction. DNA was then precipitated in ethanol and dissolved in 20 μl of TE buffer. DNA (2 μl) was used for each PCR with primers Osx-ChIP-F: 5′-GAGTGTCG-TCCCCAATCC-3′ and Osx-ChIP-R: 5′-CTGCTACCACCG-AGGCTG-3′, yielding a 120 bp product. As a negative control, another 1×10^7 mouse DPCs was treated as above, except 20 μg rabbit IgG or 10 μg goat IgG antibodies were used instead of specific antibodies. Input (diluted 1:20) was used as the positive control for PCR.

Statistics

Statistical analyses were performed using Student's unpaired *t* test. Each experiment was performed at least twice, and the representative data are presented as means ± S.D. for at least three independent replicates.

RESULTS

Expression of *Runx3*, *Runx2*, *Osterix* and *Bmp2* during tooth development

In the developing tooth, *Runx3* was detected in the dental papillae at the late cap stage (15.0 days post coitum). *Runx3* was progressively restricted to the odontoblastic layer of tooth germ from the bell stage (17.0 days post coitum) until the differentiation stage, P1 during terminal differentiation of odontoblasts (Figures 1A–1D). In contrast, *Osterix* was first detected in the odontoblastic layer at 17.0 days post coitum, and was more pronounced at P1 and P4 (Figures 1E–1H) and had overlapping expression with *Runx3*. In the odontoblasts, *Bmp2* also was strongly expressed at P1 (Figure 1O), but not *Runx2* (Figure 1K). No positive signal was detected when using sense probes.

Expression of *Runx3* and *Osterix* during differentiation of the dental pulp cells into odontoblasts *in vitro*

We next determined whether the mouse DPCs have *in vitro* expression patterns of *Runx3* and *Osterix* similar to those observed *in vivo*. RT-PCR was performed to examine gene expression of *Runx3*, *Osterix* and the odontoblast markers *Dspp* (dentin sialophosphoprotein), *enamelysin* and *KLK4* (kallikrein 4) in cell culture (Figure 2A). *Dspp* and *KLK4* were first detected clearly on day 21 and *enamelysin* on day 28, showing spontaneous differentiation of the DPCs into odontoblasts. *Runx3* expression was weakly detected on day 1, and increased further on day 21. *Osterix* expression was first detected on day 21 (Figure 2A). These results correlated with the *in vivo* expression during tooth development, suggesting that the DPCs might be useful for the study of the regulation of expression of *Osterix* by Runx3 at the stage before terminal differentiation of odontoblasts.

Runx3 down-regulates *Osterix* expression in mouse DPCs

To examine whether *Osterix* expression was regulated by Runx3, MSCV-EGFP-Flag-Runx3 was transfected by electroporation into the mouse DPCs. Electroporation, at three square-wave pulses at a frequency of 1 Hz with a pulse length of 99 μs and 1350 V, provided an optimal method for gene transfer *in vitro*. The cell

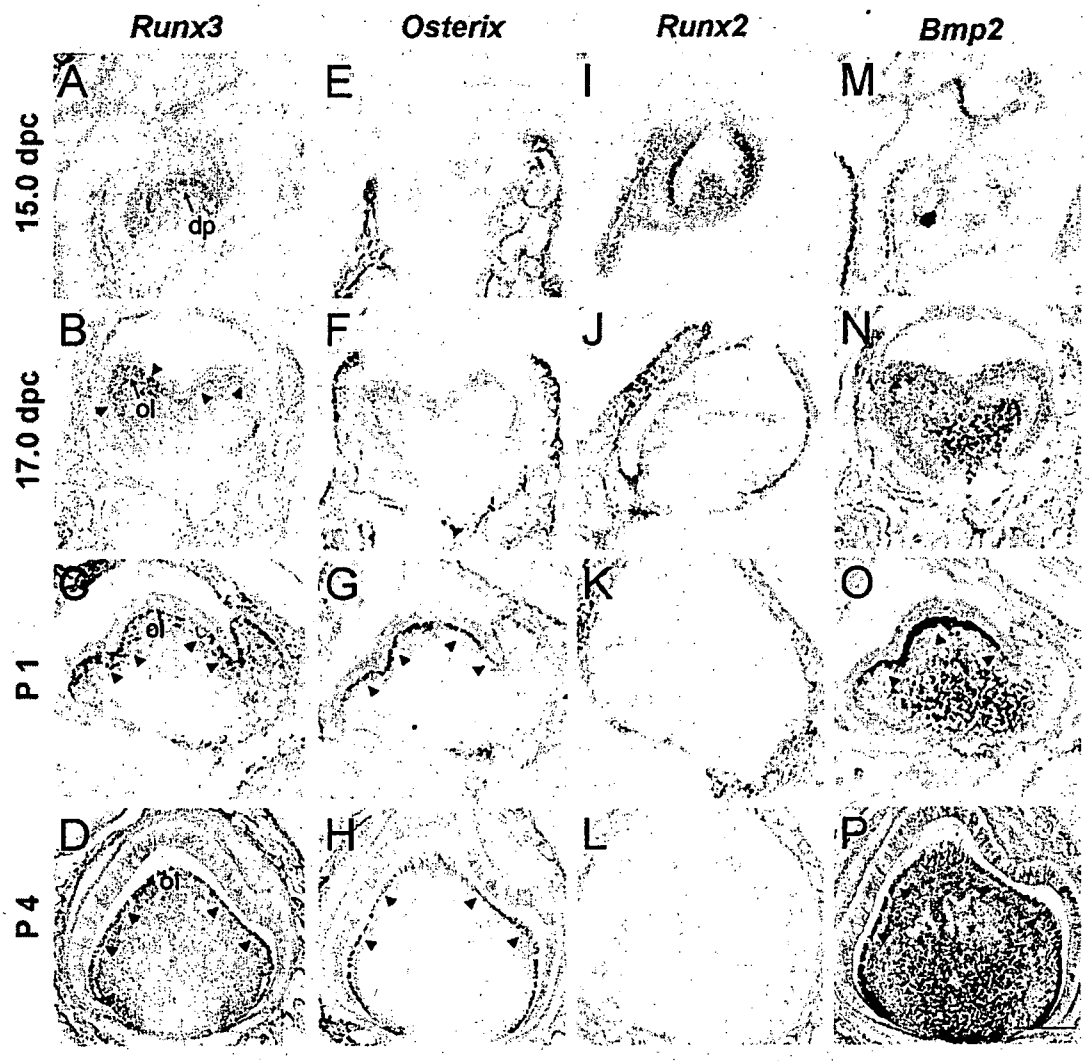

Figure 1 Expression of *Runx3*, *Osterix*, *Runx2* and *Bmp2* by *in situ* hybridization during tooth development in mouse

(**A–D**) *Runx3* was progressively restricted to the odontoblastic layer of tooth germ starting from the bell stage (17.0 days post coitum) to the differentiation stage (P1) during terminal differentiation of odontoblasts. (**E–H**) *Osterix* was first detected weakly in the odontoblastic layer at 17.0 days post coitum, and was a more pronounced at P1, overlapping with *Runx3* expression. (**I–L**) *Runx2* was not expressed in odontoblast layer after P1. (**M–P**) *Bmp2* was strongly expressed in the odontoblasts at P1. Arrowheads indicate the positive signals in the odontoblastic layer. dp, dental papillae; ol, odontoblast layer. Scale bar = 200 μm.

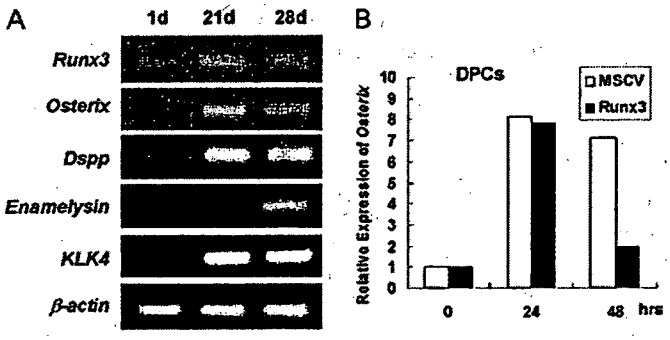

Figure 2 Down-regulation of *Osterix* expression by Runx3 in mouse DPCs *in vitro*

(**A**) mRNA expression levels for *Runx3*, *Osterix*, and for the differentiation markers of odontoblasts, *Dspp*, *enamelysin* and *KLK4* in mouse DPCs in cell culture. (**B**) *Osterix* expression was down-regulated in mouse DPCs at 48 h after *Runx3* transfection. The experiment was repeated twice with similar results.

viability was nearly 70%, as determined with Trypan Blue staining, and the efficiency was nearly 35%, as estimated by fluorescence microscopy. Real-time RT-PCR showed that the expression of *Runx3* mRNA was enhanced approx. 3-fold in DPCs transfected with MSCV-EGFP-Flag-Runx3 compared with control DPCs transfected with MSCV-EGFP after 24 h (results not shown). *Runx3* mRNA expression levels, however, were reduced to almost the same level as the control 48 h after transfection. On the other hand, *Osterix* expression was reduced by 25% 48 h after transfection with MSCV-EGFP-Flag-Runx3 compared with control transfections (Figure 2B). These results suggest that Runx3 negatively regulates *Osterix* expression in the DPCs.

Runx3 down-regulates the *Osterix* promoter activity in HEK-293 cells

A recent study has shown that *Runx2* specifically up-regulated *Osterix* promoter activity in C3H10T1/2 and ATDC5 cells, which are mesenchymal cell lines from bone and cartilage respectively

[19]. There has, so far, been no report concerning *Osterix* regulation by Runx3. Runx3 shares highly conserved DNA-binding domains with Runx2. Both the *Runx2* and the *Runx3* promoters have putative Runx-binding sites that are fully conserved in sequence and location [24], therefore cross-regulation between Runx2 and Runx3 might be plausible. To avoid this possible endogenous effect, HEK-293 cells, in which neither Runx2 nor Runx3 are expressed (Figure 3A), were used to examine transcriptional activity induced by Runx3.

Three putative Runx-binding sites were identified at positions −1823 to −1817 bp (site 1, ACCACA), −1776 to −1771 bp (site 2, ACCACT) and −713 to −707 bp (site 3, AGTGGTT) relative to the cap site by computer analysis of the *Osterix* promoter (Figure 3B). A wild-type luciferase reporter plasmid containing all the three putative Runx-binding sites was compared with the *Osterix* promoter containing five different mutations (M1–M5), in which some of the three putative sites were mutated (Figure 3B). Cells in which the wild-type reporter plasmid was co-transfected with Runx3 reduced the *Osterix* promoter activity to approx. 55%. Transfection of the mutant reporters in which site 1 and/or site 2 were mutated resulted in almost the same reduced activity as that of the wild-type promoter. In contrast, in the mutant reporters in which site 3 was mutated (M4 and M5), only a weak repression (approx. 90% activity) was detected (Figure 3B). These results suggest that site 3 is essential for *Osterix* promoter activity. To confirm this, shorter wild-type and mutant plasmids containing only site 3 were used. The *Osterix* promoter activity was significantly reduced in cells transfected with the wild-type construct, whereas the cells transfected with the mutant construct were unaffected (Figure 3C). These results suggest that site 3 is essential for *Osterix* promoter activity.

Characterization of Runx3 binding to site 3

To determine whether transcriptional repression of *Osterix* is due to direct binding of Runx3 to site 3, EMSAs using nuclear extracts from the mouse DPCs were performed. As shown in Figure 4(A), 38 bp end-labelled oligonucleotide containing the site 3 (−713 to −707 bp) of the *Osterix* promoter formed a DNA–protein complex (Figure 4A, lane 2, arrowhead). The complex was competed out completely by a 125-fold excess of unlabelled wild-type oligonucleotide (Figure 4A, lane 3). An oligonucleotide in which site 3 was mutated did not affect this binding (Figure 4A, lane 4). Furthermore, an anti-Runx3 antibody bound to the DNA–protein complex (Figure 4A, lane 5, arrow), indicating the specificity of the DNA–protein complex. No band could be detected when only nuclear extract was loaded (Figure 4A, lane 6).

Next, we performed ChIP assays to test if Runx3 binds specifically to the putative response element *in vivo*. Using mouse DPCs, proteins were cross-linked on to chromatin and immunoprecipitated with an anti-Runx3 antibody. The presence of the *Osterix* promoter DNA was detected by PCR using primers flanking site 3 (−713 to −707 bp) (Figure 4B), indicating that Runx3 binds to site 3 of *Osterix* promoter both specifically and functionally. The use of an anti-Runx2 antibody resulted in a similar result (Figure 4B), suggesting that both Runx3 and Runx2 are able to bind site 3 *in vivo*.

DISCUSSION

During a systematic *in situ* hybridization study of tooth development, *Osterix* mRNA was first detected in terminally differentiating odontoblasts and showed co-localization with *Runx3*, suggesting a potential role for both genes in odontoblast differentiation. Runx3 overexpression resulted in down-regulation

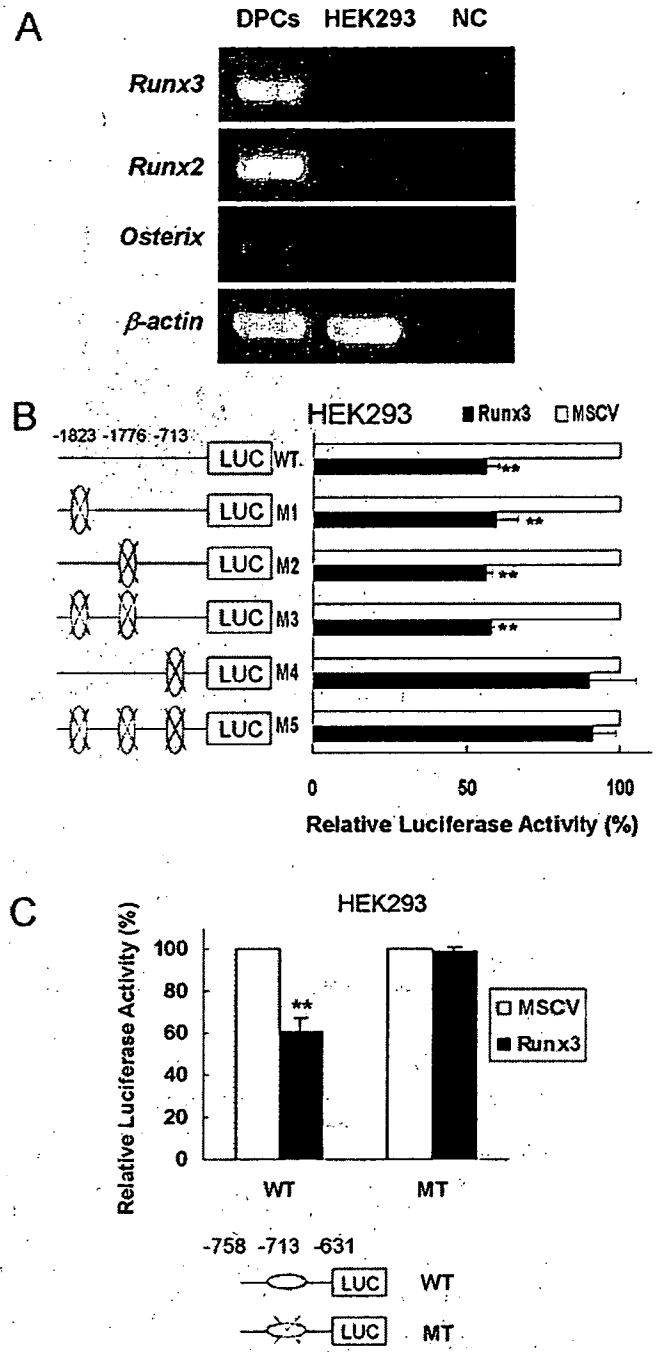

Figure 3 Down-regulation of *Osterix* promoter activity by Runx3 in HEK-293 cells

(**A**) Determination of endogenous expression levels of *Runx3*, *Runx2* and *Osterix* in mouse DPCs and HEK-293 cells. (**B**) Wild-type (WT) and mutant (MT) *Osterix* promoter plasmids were analysed 48 h after co-transfection with MSCV-EGFP-Flag-Runx3 into HEK293 cells. (**C**) Shortened wild-type (WT) or mutant (MT) *Osterix* promoter plasmids containing only site 3 (−713 to −707) were co-transfected with MSCV-EGFP-Flag-Runx3 into HEK-293 cells. The activities were determined after 48 h and normalized against the co-transfected internal control plasmid (pRL-SV40). The values represent means ± S.D. for four individual samples. The experiment was repeated twice with similar results. **, $P < 0.01$ compared with the empty MSCV plasmid. NC, negative control.

of *Osterix* in the mouse DPCs. This suggests that *Osterix* might be a downstream target of *Runx3* in tooth development. *Osterix* null mice [18] have a similar phenotype to the *Runx2* null mice [9,10], in which both intramembranous and endochondral bone are not

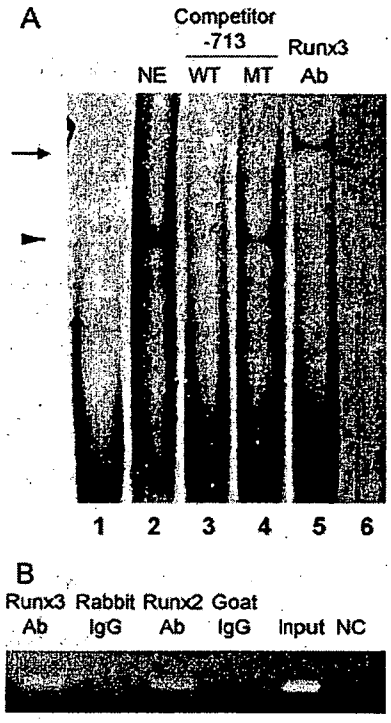

Figure 4 Characterization of Runx3 binding to the *Osterix* promoter by EMSA and ChIP assay

(**A**) Interaction of nuclear extract (NE) of mouse DPCs with *Osterix* promoter −713 to −707 bp sequence (site 3) in EMSA. The arrowhead indicates the retarded protein–DNA complexes. The arrow indicates the super-shift band in the reaction with the addition of an anti-Runx3 antibody (lane 5). Lane 1 shows a binding reaction with no protein. Lane 2 is a control reaction with no competing oligonucleotides. Lanes 3 and 4 represent competition reactions with wild-type (WT) or mutated (MT) unlabelled oligonucleotides. Lane 6, nuclear extract only. (**B**) ChIP assays were performed to investigate whether both Runx3 and Runx2 could bind to the *Osterix* promoter *in vivo*. A 120-bp band could be detected by PCR in both anti-Runx3 and anti-Runx2 antibody treated samples, but not in anti-rabbit or anti-goat IgG treated samples. Ab, antibody; NC, negative control.

formed due to the lack of osteoblast differentiation. Whereas *Osterix* is not expressed in the *Runx2* null mutants, *Runx2* expression is not changed in the *Osterix* null mutants [18]. These genetic studies have placed *Osterix* downstream of *Runx2* [18]. The precise regulatory role of Runx2 in *Osterix* expression is not clear. A recent study has shown that a 737 bp fragment of the *Osterix* promoter is up-regulated upon *Runx2* overexpression in ATDC5 chondroprogenitor cells, and the function of the 737 bp fragment was confirmed by site-directed mutagenesis experiments [19]. Furthermore, this functional binding site is conserved among mouse, rat and human, showing conservation of the DNA-binding site [19]. However, no information is available on the regulation of *Osterix* expression by Runx3. Therefore, we have performed transient co-transfection, EMSAs and ChIP assays to investigate the relationship between Runx3 and Osterix in DPCs. Structural dissection of the proximal promoter of the *Osterix* gene revealed the presence of three putative Runx-binding sites. Only site 3 (−713 to −707 bp) of the identified sites was preferentially and functionally occupied by Runx3. The disruption of site 3 leads to increased *Osterix* promoter activity in HEK-293 cells, in which both Runx2 and Runx3 are not expressed endogenously. These results indicate that *Osterix* expression is negatively regulated by Runx3. Furthermore, our EMSAs and ChIP assays confirmed that Runx3 directly down-regulates *Osterix* expression in DPCs prior to terminal differentiation into odontoblasts. It is noteworthy that Runx3 negatively regulates *CD36* expression in myeloid cells [25] and suppresses gastric epithelial cell growth [26], implying a general role for Runx3 in transcriptional repression.

The distinct roles of Runx2 and Runx3 in odontoblast differentiation are not clear. Previous research indicated that tooth development was disrupted in the cap/early bell stages in the *Runx2* null mice and no overt differentiation of odontoblasts was observed [11,27]. There was no conspicuous phenotype in teeth of *Runx3* null mice [17]. In *Runx2* null mice, *Runx3* expression was enhanced dramatically in the mesenchyme of upper molars, and they differentiated into odontoblasts [27]. Our EMSAs and ChIP assays have shown that not only Runx2, but also Runx3 binds to site 3 of the *Osterix* promoter. *Runx3* overexpression resulted in down-regulation of *Osterix* in DPCs. The *Osterix* promoter activity was down-regulated by *Runx3* transfection in HEK-293 cells. These results suggest that *Osterix* expression is co-operatively regulated by Runx2 and that Runx3 is sharing the same binding site on the *Osterix* promoter. Thus, Runx3 might co-operate with Runx2 to regulate *Osterix* expression during odontoblast differentiation. The role of Osterix in tooth development is not clear. In skeletal development, Runx2, Runx3 and Osterix play pivotal roles in osteoblast differentiation and hypertrophic chondrocyte maturation [28,29]. Osterix may play a role in segregation of osteoblast and chondrocyte lineages [29,30]. *Runx2* and *Runx3* are co-expressed in the early stages of tooth development. There is overlapping expression of *Osterix* with *Runx3*, but not with *Runx2* in terminal differentiation of odontoblasts. Therefore *Osterix* may play a role in lineage commitment of odontoblasts in tooth development. The diverse transcriptional outcomes of Runx activity are dependent on context [1]. The Runx family members act as organizing factors on the promoters of target genes, where they associate with co-activators and other DNA-binding transcription factors, including Smads [1]. Repression of *Osterix* by Runx3 in DPCs is an example of context-dependent regulation of lineage commitment. Thus, there might be co-operative interactions among BMPs, Smads, Runx2 and Runx3 in the regulation of *Osterix* expression during DPC differentiation into odontoblasts.

We thank Professor A. Akamine (Department of Dental Science, Faculty of Dental Science, Kyushu University, Fukuoka, Japan) for his help. This work was supported by a Grant-in-Aid for Scientific Research from the Ministry of Education, Science, Sports and Culture, Japan, #17390509 and #18-06588.

REFERENCES

1 Durst, K. L. and Hiebert, S. W. (2004) Role of RUNX family members in transcriptional repression and gene silencing. Oncogene **23**, 4220–4224
2 Ito, Y. (2004) Oncogenic potential of the RUNX gene family: 'overview'. Oncogene **23**, 4198–4208
3 van Wijnen, A. J., Stein, G. S., Gergen, J. P., Groner, Y., Hiebert, S. W., Ito, Y., Liu, P., Neil, J. C., Ohki, M. and Speck, N. (2004) Nomenclature for Runt-related (RUNX) proteins. Oncogene **23**, 4209–4210
4 Bangsow, C., Rubins, N., Glusman, G., Bernstein, Y., Negreanu, V., Goldenberg, D., Lotem, J., Ben-Asher, E., Lancet, D., Levanon, D. and Groner, Y. (2001) The *RUNX3* gene–sequence, structure and regulated expression. Gene **279**, 221–232
5 Levanon, D., Glusman, G., Bangsow, T., Ben-Asher, E., Male, D. A., Avidan, N., Bangsow, C., Hattori, M., Taylor, T. D., Taudien, S. et al. (2001) Architecture and anatomy of the genomic locus encoding the human leukemia-associated transcription factor RUNX1/AML1. Gene **262**, 23–33
6 Ogawa, E., Maruyama, M., Kagoshima, H., Inuzuka, M., Lu, J., Satake, M., Shigesada, K. and Ito, Y. (1993) PEBP2/PEA2 represents a family of transcription factors homologous to the products of the *Drosophila runt* gene and the human *AML1* gene. Proc. Natl. Acad. Sci. U.S.A. **90**, 6859–6863
7 Thirunavukkarasu, K., Mahajan, M., McLarren, K. W., Stifani, S. and Karsenty, G. (1998) Two domains unique to osteoblast-specific transcription factor Osf2/Cbfa1 contribute to its transactivation function and its inability to heterodimerize with Cbfβ. Mol. Cell. Biol. **18**, 4197–4208

8 Komori, T. (2005) Regulation of skeletal development by the Runx family of transcription factors. J. Cell. Biochem. **95**, 445–453
9 Komori, T., Yagi, H., Nomura, S., Yamaguchi, A., Sasaki, K., Deguchi, K., Shimizu, Y., Bronson, R. T., Gao, Y. H., Inada, M. et al. (1997) Targeted disruption of Cbfα1 results in a complete lack of bone formation owing to maturational arrest of osteoblasts. Cell **89**, 755–764
10 Otto, F., Thornell, A. P., Crompton, T., Denzel, A., Gilmour, K. C., Rosewell, I. R., Stamp, G. W., Beddington, R. S., Mundlos, S., Olsen, B. R. et al. (1997) Cbfα1, a candidate gene for cleidocranial dysplasia syndrome, is essential for osteoblast differentiation and bone development. Cell **89**, 765–771
11 D'Souza, R. N., Aberg, T., Gaikwad, J., Cavender, A., Owen, M., Karsenty, G. and Thesleff, I. (1999) Cbfα1 is required for epithelial-mesenchymal interactions regulating tooth development in mice. Development **126**, 2911–2920
12 Ducy, P., Zhang, R., Geoffroy, V., Ridall, A. L. and Karsenty, G. (1997) Osf2/Cbfα1: a transcriptional activator of osteoblast differentiation. Cell **89**, 747–754
13 Mundlos, S., Otto, F., Mundlos, C., Mulliken, J. B., Aylsworth, A. S., Albright, S., Lindhout, D., Cole, W. G., Henn, W., Knoll, J. H. et al. (1997) Mutations involving the transcription factor CBFA1 cause cleidocranial dysplasia. Cell **89**, 773–779
14 Li, Q. L., Ito, K., Sakakura, C., Fukamachi, H., Inoue, K., Chi, X. Z., Lee, K. Y., Nomura, S., Lee, C. W., Han, S. B. et al. (2002) Causal relationship between the loss of RUNX3 expression and gastric cancer. Cell **109**, 113–124
15 Levanon, D., Bettoun, D., Harris-Cerruti, C., Woolf, E., Negreanu, V., Eilam, R., Bernstein, Y., Goldenberg, D., Xiao, C., Fliegauf, M. et al. (2002) The Runx3 transcription factor regulates development and survival of TrkC dorsal root ganglia neurons. EMBO J. **21**, 3454–3463
16 Brenner, O., Levanon, D., Negreanu, V., Golubkov, O., Fainaru, O., Woolf, E. and Groner, Y. (2004) Loss of Runx3 function in leukocytes is associated with spontaneously developed colitis and gastric mucosal hyperplasia. Proc. Natl. Acad. Sci. U.S.A. **101**, 16016–16021
17 Yamashiro, T., Aberg, T., Levanon, D., Groner, Y. and Thesleff, I. (2002) Expression of Runx1, -2 and -3 during tooth, palate and craniofacial bone development. Mech. Dev. **119** (Suppl. 1), S107–S110
18 Nakashima, K., Zhou, X., Kunkel, G., Zhang, Z., Deng, J. M., Behringer, R. R. and de Crombrugghe, B. (2002) The novel zinc finger-containing transcription factor Osterix is required for osteoblast differentiation and bone formation. Cell **108**, 17–29
19 Nishio, Y., Dong, Y., Paris, M., O'Keefe, R. J., Schwarz, E. M. and Drissi, H. (2006) Runx2-mediated regulation of the zinc finger Osterix/Sp7 gene. Gene **372**, 62–70
20 Platt, K. A., Michaud, J. and Joyner, A. L. (1997) Expression of the mouse *Gli* and *Ptc* genes is adjacent to embryonic sources of hedgehog signals suggesting a conservation of pathways between flies and mice. Mech. Dev. **62**, 121–135
21 Iohara, K., Zheng, L., Ito, M., Tomokiyo, A., Matsushita, K. and Nakashima, M. (2006) Side population cells isolated from porcine dental pulp tissue with self-renewal and multipotency for dentinogenesis, chondrogenesis, adipogenesis, and neurogenesis. Stem Cells **24**, 2493–2503
22 Schreiber, E., Matthias, P., Muller, M. M. and Schaffner, W. (1989) Rapid detection of octamer binding proteins with 'mini-extracts', prepared from a small number of cells. Nucleic Acids Res. **17**, 6419
23 Bradford, M. M. (1976) A rapid and sensitive method for the quantitation of microgram quantities of protein utilizing the principle of protein–dye binding. Anal. Biochem. **72**, 248–254
24 Drissi, H., Luc, Q., Shakoori, R., Chuva De Sousa Lopes, S., Choi, J. Y., Terry, A., Hu, M., Jones, S., Neil, J. C., Lian, J. B. et al. (2000) Transcriptional autoregulation of the bone related CBFA1/RUNX2 gene. J Cell Physiol **184**, 341–350
25 Puig-Kroger, A., Dominguez-Soto, A., Martinez-Munoz, L., Serrano-Gomez, D., Lopez-Bravo, M., Sierra-Filardi, E., Fernandez-Ruiz, E., Ruiz-Velasco, N., Ardavin, C., Groner, Y. et al. (2006) RUNX3 negatively regulates CD36 expression in myeloid cell lines. J. Immunol. **177**, 2107–2114
26 Chi, X. Z., Yang, J. O., Lee, K. Y., Ito, K., Sakakura, C., Li, Q. L., Kim, H. R., Cha, E. J., Lee, Y. H., Kaneda, A. et al. (2005) RUNX3 suppresses gastric epithelial cell growth by inducing $p21^{WAF1/Cip1}$ expression in cooperation with transforming growth factor β-activated SMAD. Mol. Cell Biol. **25**, 8097–8107
27 Aberg, T., Cavender, A., Gaikwad, J. S., Bronckers, A. L., Wang, X., Waltimo-Siren, J., Thesleff, I. and D'Souza, R. N. (2004) Phenotypic changes in dentition of Runx2 homozygote-null mutant mice. J. Histochem. Cytochem. **52**, 131–139
28 Yoshida, C. A. and Komori, T. (2005) Role of Runx proteins in chondrogenesis. Crit. Rev. Eukaryot. Gene Expr. **15**, 243–254
29 Komori, T. (2006) Regulation of osteoblast differentiation by transcription factors. J. Cell. Biochem. **99**, 1233–1239
30 Nakashima, K. and de Crombrugghe, B. (2003) Transcriptional mechanisms in osteoblast differentiation and bone formation. Trends Genet. **19**, 458–466

Received 18 January 2007/19 February 2007; accepted 13 March 2007
Published as BJ Immediate Publication 13 March 2007, doi:10.1042/BJ20070104

●特別企画

HERS

歯科再生医療はどこまで到達し，どこへ向かうのか？

●歯根再生のキーワードとしての「HERS」のメカニズムに迫る

大島勇人[1]・藤原尚樹[2]・Han-Sung Jung[3]・太田正人[4]・齋藤正寛[5]・原田英光[2]

歯科再生医療研究は，何がどこまで進んでいて，今後どのような展開が待っているのだろうか？

第49回歯科基礎医学会学術大会・サテライトシンポジウム「ヘルトヴィッヒの上皮鞘（HERS）と歯根発生のバイオロジー」では，歯科再生医療では，補綴処置が可能な歯冠の再生以上に，歯根の再生を視野に入れる必要があり，そこでは「ヘルトヴィッヒの上皮鞘（HERS）」形成のメカニズムの解明がキーワードになることが示された．

本特別企画では，当日のシンポジストによる最新知見の報告をダイジェストにてお届けするとともに，歯科再生医療の現状と今後の展開について俯瞰していただく．

（編集部）

1) 新潟大学大学院医歯学総合研究科顎顔面再建学講座硬組織形態学分野
〒951-8514　新潟市中央区学校町通2-5274
Tel.025-227-2812　E-mail.histoman@dent.niigata-u.ac.jp
2) 岩手医科大学歯学部口腔解剖学第二講座
3) 延世大学校歯科大学口腔生物学講座組織学分野（Division in Anatomy and Developmental Biology, Department of Oral Biology, Research Center for Orofacial Hard Tissue Regeneration, Brain Korea 21 Project, Yonsei University College of Dentistry, Seoul, Korea）
4) 東京医科歯科大学大学院医歯学総合研究科顎顔面機構制御学講座部分子発生学分野
5) 大阪大学大学院歯学研究科口腔分子免疫制御学講座生化学分野

歯科再生医療の現状——なぜいま「HERS」なのか？

大島勇人　Hayato Oshima
新潟大学大学院医歯学総合研究科顎顔面再建学講座硬組織形態学分野　E-mail:histoman@dent.niigata-u.ac.jp

◎歯科再生医療のこれまでと，現状での到達点

歯がつくられる過程（歯の発生）は，腎臓や肺などがつくられるのと同じように，上皮[註1]と間葉[註2]間の相互作用（上皮間葉相互作用[註3]）で進行します．この過程で，顎の特定の場所に歯がつくられ始め，切歯・犬歯・臼歯など，その場に応じた歯が形づくられた後に，硬い歯の組織（象牙質やエナメル質）がつくられます．この上皮間葉相互作用において，ツールキット遺伝子[註4]と呼ばれるシグナルがとても重要な役割を果たすことが明らかになっています．

現在，歯の再生に向けてどのような取り組みがなされているかというと，「からだ」から歯をつくる種となる細胞（幹細胞）を取り出して，「からだ」に馴染みやすい材料の助けで，取り出した細胞を歯の細胞に誘導し歯をつくる試み（組織工学的歯の再生）です．現在，生まれる前のネズミの歯胚[註5]や生後のブタの親知らずの細胞を使った歯の再生が成功しており，歯をつくる細胞さえ入手できれば，ヒトでも歯の再生が可能であることを示しています．

◎歯冠再生なのか？　歯根再生なのか？

歯胚から取り出した細胞を使って組織工学的に歯を再生させることは可能になりましたが，歯の再生へ向けて克服しなければならない問題が数多く残されています．問題点の一つとして，再生歯の形をどうつくるかがあげられます．組織工学的歯の再生においては，しばしば歯牙腫[註6]様の再生歯が形成され，再生歯の形や数をコントロールすることが難しいのが現状です．歯の形や数の制御が可能になったとしても，歯は，食事をしたり，声を出したりするだけでなく，審美的な要求にも応えなければなりませんので，補綴処置などの従来からの歯科医療技術の助けが必要になります．このことは，歯の数のコントロールは克服しなければならなりませんが，歯の形の問題は歯科医療技術の助けで解決できると言えるでしょう．一方，歯が口の中で機能するためには，歯周組織の再生が必要となります．言い換えれば，歯冠再生が実現しても，歯根再生を実現しなければ，歯の再生技術が歯科医療に応用できないことになります．

◎なぜ「HERS」が注目されるのか？

歯の発生は上皮間葉相互作用により進行しますが，この過程は特定の場所に歯の芽がつくられ（誘導），歯胚が形づくられ（形態形成），硬い組織になる（細胞分化と基質形成）というステップを踏んで歯冠がつくられます（**図1**）．

歯の芽がつくられる前には，顎には馬蹄形の上皮の高まり（歯堤）がつくられ，その後に特定の場所に歯の芽である歯胚がつくられます．歯胚の上皮は蕾状，帽子状，釣り鐘状を呈し，それぞれ蕾状期歯胚，帽状期歯胚，鐘状期歯胚と呼ばれます．引き続いて，将来の咬頭頂となる部分から歯が硬くなり始めます（象牙芽細胞とエナメル芽細胞への分化と象牙質とエナメル質の形成）．

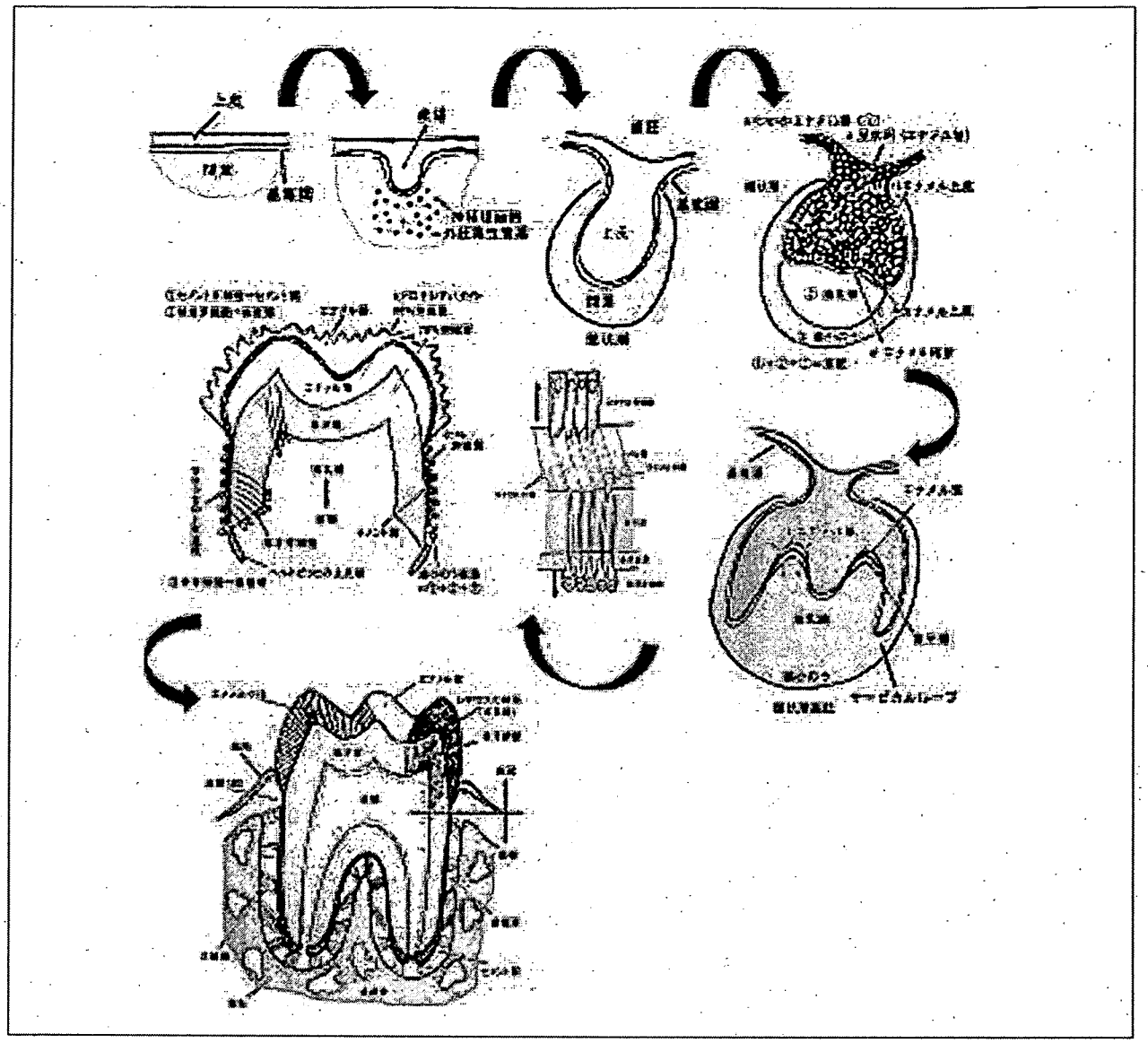

図1　歯の発生過程

歯の発生は上皮間葉相互作用で進行するが，上皮と間葉の間には基底膜が存在する．顎には馬蹄形の上皮の高まり（歯堤）がつくられ，その後に特定の場所に歯の芽である歯胚がつくられる．歯胚は上皮（エナメル器）と神経堤註7）由来の間葉（歯乳頭と歯小嚢）から構成され，上皮の折れ返りの部分をサービカルループと呼ぶ．歯胚は雷状期，帽状期，鐘状期を経て，将来の咬頭頂となる部分から歯が硬くなり始める（象牙芽細胞とエナメル芽細胞への分化と象牙質とエナメル質の形成）．歯冠が完成すると，サービカルループがヘルトビッヒの上皮鞘（HERS）となり，歯根がつくられ始める．HERSが断裂すると，歯小嚢細胞がセメント芽細胞となりセメント質を形成し，歯根膜，歯槽骨を含めた歯周組織の形成が進行する．断裂したHERSはマラッセの上皮遺残として歯根膜中に残存する．歯が萌出すると，上皮と歯肉が繋がり，エナメル質の形成細胞は消失する

歯冠が完成すると歯根がつくられ始めますが，この歯根がつくられる過程で重要な役割を果たすのがヘルトビッヒの上皮鞘（Hertwig's epithelial root sheath，HERS）と呼ばれる上皮の存在です．歯冠がつくられる時期には，上皮と間葉の間に象牙質とエナメル質がつくられますが，その後エナメル質はつくられなくなります．このエナメル質をつくらない上皮をHERSと呼びます．つまり，HERSと間葉の相互作用により歯根がつくられるとともに，セメント質や歯根膜などの歯周組織がつくられ始めるのです（**図1**）．

しかしながら，HERSがどのようにつくられるのか？　HERSがどのような役割を担っているのか？　そしてHERSの運命はどうなるのか？　については，よくわかっていないのが現状です．

しかしながら，2005年以降，歯根発生に関する重要な論文が日本・韓国から発信されています．そこで本企画では，これらの論文の執筆者の先生方に，独自の研究手法を用いたHERSや歯根発生についてのデータを紹介していただき，HERSや歯根発生メカニズムに関する最新の知見を紹介するとともに，今後の再生医療の方向性について俯瞰することとしたい．藤原尚樹先生とHan-Sung Jung先生からは器官培養系を用いた研究成果について，それぞれHERSの分化と形成へのEGFとIGF-Iの役割，上皮間葉相互作用の観点から見た歯根形成におけるBMPの役割についての知見を紹介していただきます．太田正人先生からは遺伝子変異マウスを用いた研究成果をもとに，歯根形成におけるShhシグナル経路について概説いただきます．また，斎藤正寛先生からはヒト歯根膜形成に関わる遺伝子データベースの結果について，原田英光先生からは歯冠形成から歯根形成に移行するメカニズムの仮説について紹介いただきます．

◉最新知見の意味するもの

歯根がつくられる過程のメカニズムの研究が立ち後れている原因は，研究手法に制限があるからです．歯の発生を機能の側面から研究するために，「ある機能が失われるとどうなるか？（機能喪失）」と「ない機能を得るとどうなるか？（機能獲得）」の実験を行います．「機能喪失」とは，遺伝子レベルまたはタンパク質レベルで機能を働かなくする手法であり，「機能獲得」とは，通常は発現しない，もしくは発現が低い遺伝子を強く発現させたり，またはタンパク質をたくさん作用させたりする手法です．このような手法は，細胞レベルから動物固体レベルまで機能を調べることができますが，培養実験を確立したり遺伝子改変動物をつくったりして，どのような異常が起こるかを解析することが必要になります．ツールキット遺伝子欠損動物の解析では，動物が生後にすぐに死んでしまうものが多く，生後に始まる歯根形成の解析を難しくしています．また，歯根形成は周囲の歯槽骨形成と連動して進行するため，歯周組織形成を培養実験系で確立する必要があります．

本企画で紹介する各研究は，上記の問題を解決するために，独自の手法を駆使して歯根発生メカニズムの解析に成功している研究であり，世界からも注目を浴びている研究成果です．

註1) 上皮とは，体表・体腔・管腔構造をつくる組織で，通常細胞同士が敷石状に密に接触し合う特徴をもつ

註2) 上皮以外の組織を間葉といい，細胞間が広く開いた構造を示すのが特徴である

註3) 上皮と間葉間の時間的・空間的相互作用を上皮間葉相互作用という

註4) 生物種にかかわらず，形づくりには複数の遺伝子が一つのセットとして働くことから，この共通の「遺伝子という道具箱（ツールキット）」をツールキット遺伝子と呼ぶ．骨形態形成因子（BMP），線維芽細胞増殖因子（FGF），ウィント（Wnt），ソニックヘッジホッグ（Shh），腫瘍壊死因子（TNF）などが知られている

註5) 将来歯となる歯の芽を歯胚といい，上皮と間葉からなる

註6) 大小さまざまな変形した歯が形成される腫瘍の一種

註7) 脳や脊髄の原基である神経管がつくられる時に，神経管になる上皮と皮膚になる上皮の境界にある細胞群を神経堤細胞と呼び，間葉へ遊走し歯をつくる間葉細胞となる

注目の研究

【器官培養系を用いた歯根形成メカニズムの解明】

藤原尚樹　Naoki Fujiwara
岩手医科大学歯学部口腔解剖学第二講座／E-mail:naokif@iwate-med.ac.jp

歯冠形成から歯根形成へ移行する際，エナメル器の下端では星状網（SR）が消失し，内エナメル上皮（IEE）と外エナメル上皮（OEE）の二層からなるヘルトヴィッヒの上皮鞘（HERS）が分化する．この過程でサービカルループから上皮成長因子（EGF）受容体の発現が免疫組織学的に消失する一方で，インスリン様成長因子（IGF）-I受容体はHERSに発現することが判明した．

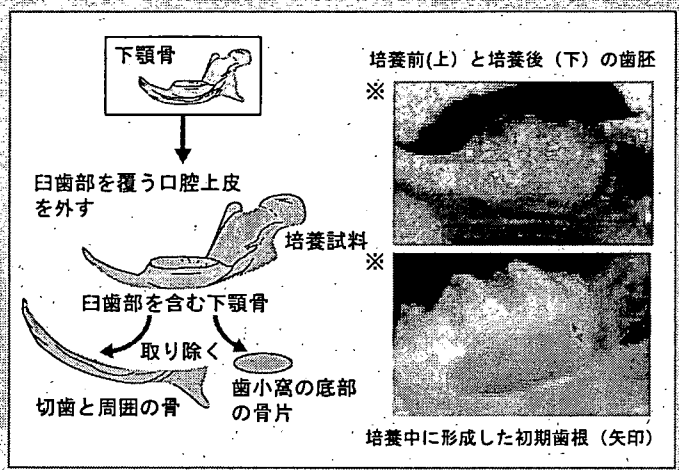

図1　生後臼歯歯胚の器官培養

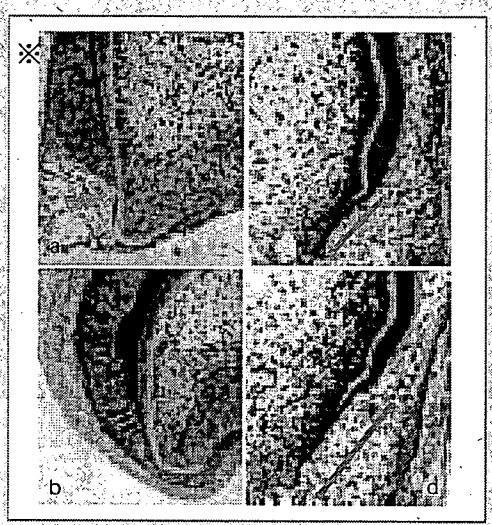

図2　器官培養における歯胚への成長因子の影響
a,b：生後3日齢臼歯歯胚2週間培養．a-対照群，b-EGF添加群．
対照群ではHERSが断裂し（矢印），初期歯根形成がみられるが，EGF添加群では星条網（※）が消失せず，エナメル質形成が継続している
c,d：生後5日齢臼歯歯胚4日間培養．c-対照群，d-IGF-1添加群．対照群のHERS（ライン）は発達するが短いのに対し，IGF-1添加群ではHERSが伸長し，歯根形成が促進されている

われわれが考案した器官培養系（図1）は，歯胚の他に歯根膜と骨も保持しており，生後マウス臼歯歯胚の発達を観察することができる．この系を用いた実験（図2）から，このSRの消失にはEGFが調節因子として関わっており，IGF-IはHERSのOEEの細胞増殖活性を促進することで，HERSの伸長を促進することがわかった．これまで不明であったHERSの分化と形成にEGFとIGF-Iが，それぞれ時期特異的に重要な役割を果たすことが示された．

この知見，どう読めばよい？

本研究の注目すべき点は，歯根形成メカニズムを解析するためのエレガントな実験系を確立したことです．この実験系を使って，歯冠形成から歯根形成に移行するタイミングが二種類の成長因子（EGFとIGF-I）の発現を切り替えることによって決定されることを明らかにしています．歯がつくられている時期，に二種類の成長因子を「からだ」に時期を変えて投与することにより，歯冠と歯根の長さを調節するようなことが，将来実現できるかも知れません．

注目の研究 ②

【Epithelial-mesenchymal interaction of Hertwig's epithelial root sheath during root formation】

Han-Sung Jung

Division in Anatomy and Developmental Biology, Department of Oral Biology, Research Center for Orofacial Hard Tissue Regeneration, Brain Korea 21 Project, Yonsei University College of Dentistry, Seoul, Korea／E-mail:hsjung@yumc.yonsei.ac.kr

歯冠形成過程において上皮間葉相互作用が重要な役割をもつことはよく知られているが，歯根形成期においてもHERSと歯乳頭および歯小嚢間に相互作用が存在すると考えられる．個体発生において多様な機能をもつBMP4は，歯冠形成期ではサービカルループ周囲に局在しないが（図1a），歯根形成期になるとHERS周囲の間葉細胞で局在を示している（図1b）．

そこでわれわれは，HERS形成におけるBMP4の役割を検討する目的で，BMP4およびBMP阻害作用をもつNogginビーズを歯根形成期のマウス歯乳頭に移植した．移植48時間後，BMP4群において有意にHERSの伸張およびPCNA陽性細胞数の増加が認められた．またNoggin群ではHERSの発育は抑制された（図2）ことから，HERS周囲の間葉細胞が分泌するBMP4は，HERSの成長を促進する可能性が示された．したがって，BMP4は歯根形成を正に調節する因子として，再生工学における応用が期待される．

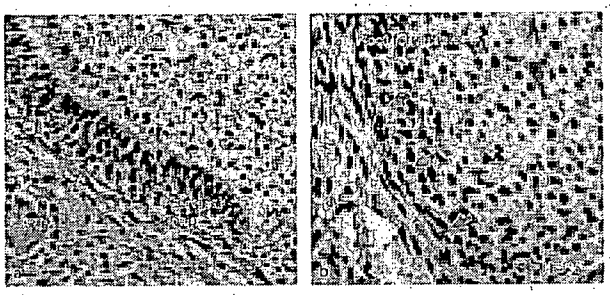

図1　歯冠形成期（a）および歯根形成期（b）におけるHERS周囲のBMP4局在の有無

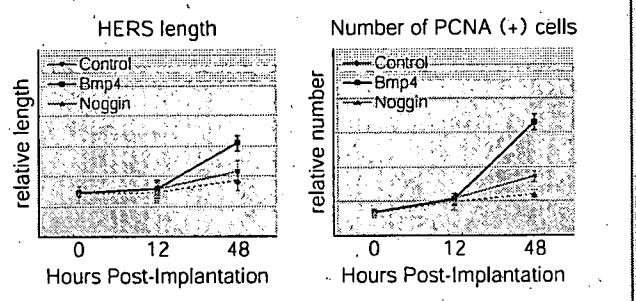

図2　HERS形成におけるBMP4の役割

この知見，どう読めばよい？

本研究で注目すべき点は，器官培養系にビーズ実験[註8)]を応用することにより，BMPの役割を解明したことです．ここでは，BMPがアクセル，Nogginがブレーキの役割をしているので，二種類のタンパク質のアクセルとブレーキの作用をうまく利用できれば，歯根の長さを自由に調節できるようになるのも夢ではありません．

註8）タンパク質を滲みこませたビーズを器官培養系に作用させることにより，タンパク質の機能獲得の条件をつくり出せる．また逆に，タンパク質の阻害薬を作用させると機能喪失の条件をつくり出せる

注目の研究

【歯根発生におけるソニックヘッジホッグ（Shh）経路の役割】

太田正人　Masato Ota
東京医科歯科大学大学院医歯学総合研究科顎顔面機構制御学講座部分子発生学分野／E-mail:seijin.emb@tmd.ac.jp

脊椎動物の「体づくり」の過程で重要な役割を果たすソニックヘッジホッグ（Shh）経路は，胎生期の歯胚上皮においても細胞増殖や細胞死を制御し，臼歯の歯冠形態を決定する（図1）．

このShhシグナル経路が歯根の形態形成にも関与する可能性を検証するため，マウス臼歯の歯根形成過程におけるShhシグナル経路遺伝子の発現パターンを調べた結果，歯根発生に重要なHERS や周囲の歯乳頭増殖帯で遺伝子発現を観察した．次にShh受容体のPatched1（Ptc1）遺伝子に変異をもちShhシグナル経路に異常のあるPtc1 mes遺伝子変異マウスを解析した．Ptc1 mesでは，生後1週齢でHERS周囲の増殖帯での増殖活性の低下，また生後4週齢で臼歯の萌出遅延と歯根伸長不全（図2a），さらにFGF-2，FGF-18の発現低下が観察された（図2b）．現在，このようにFGFsを介したShhによる臼歯の歯根発生の制御機構が明らかにされつつある．

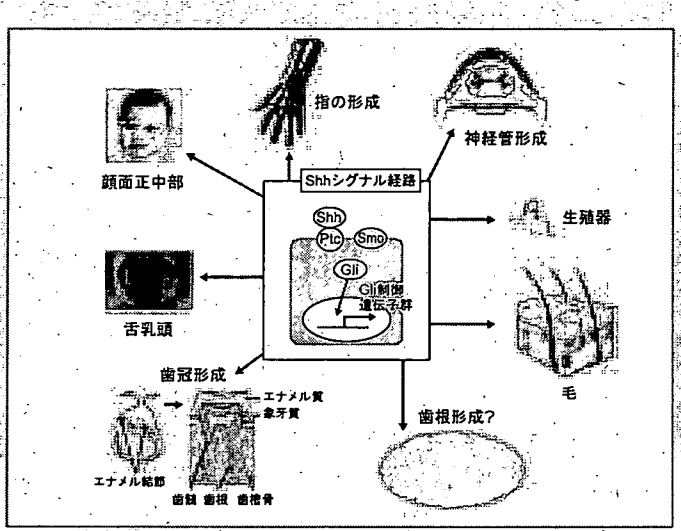

図1「からだ」づくりにおけるshh経路

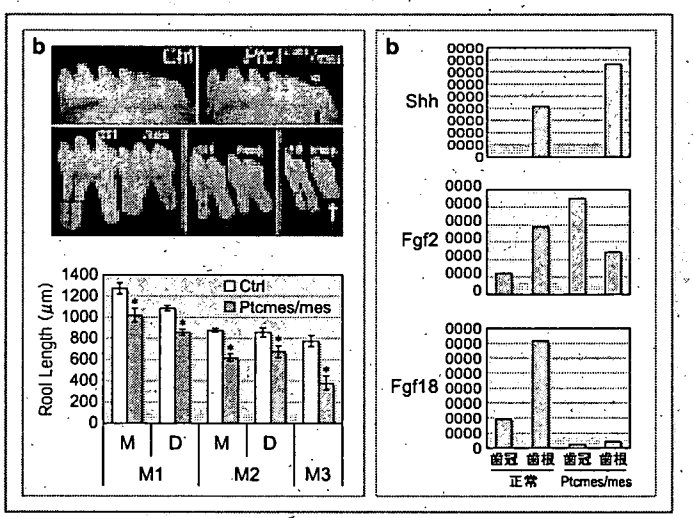

図2　歯根形成過程におけるshhシグナル経路遺伝子発現パターン

この知見，どう読めばよい？

本研究の注目すべき点は，歯冠形成で重要な働きをするShhの歯根形成における役割を示したことです．Shhがうまく働かないと，萌出が遅れ歯根が短くなることから，歯根形成にShhが重要な役割を果たすことが示されています．Shhがうまく働かないと，連動して他のシグナル（FGF）が抑制されるように，「からだ」では一つのシグナルがおかしくなると，関連したシグナルにも影響することがわかります．将来の歯根の長さや数の調整には，Shhシグナルをうまく操れるようになることが必要であると言えます．